Sedimentary Geology 424 (2021) 105982

Contents lists available at ScienceDirect

Sedimentary Geology

journal homepage: www.elsevier.com/locate/sedgeo

Controls on the compositional framework and petrogenesis of Early Cretaceous first cycle quartzose sandstone, North Gondwana

Mohammed Mashre Atman Ahfaf [a], Ekundayo Joseph Adepehin [a,*], Che Aziz Ali [a], Habibah Jamil [a], Sylvester Powei Lubi [b]

[a] Basin Research Group, Department of Earth and Environmental Sciences, Faculty of Science and Technology, The National University of Malaysia, Bangi, Selangor, Malaysia
[b] Department of Applied Geology, The Federal University of Technology Akure, Nigeria

ARTICLE INFO

Article history:
Received 21 May 2021
Received in revised form 12 August 2021
Accepted 15 August 2021
Available online 10 September 2021

Editor: Dr. Jasper Knight

Keywords:
Syn-rift sediments
Quartzarenite
Provenance
Humid paleoclimate
Northern Gondwana, tectonic setting

ABSTRACT

Recent advances in sedimentary research have shown that quartz sandstones are scarce in the global geologic record and prolonged sediment transport does not automatically produce mineralogically mature sediments. Published data are based mainly on Cambro-Ordovician arenites. This paper discusses the formational controls of early Cretaceous syn-rift quartzose from northern Gondwana based on integrated petrographic, mineralogic, and electrofacies proxies on the Upper Sarir Sandstone Formation, Sirte Basin, Libya. The study aimed to understand the compositional framework and construe the sedimentological processes that produced the quartz-rich sandstones. Acquired samples (n = 40) from three boreholes (N8-97, N7-97, and N4-97) were subjected to petrographic analysis, x-ray diffractometry, and variable pressure scanning electron microscopy with energy dispersive x-ray spectrometry. Qualitative and quantitative datasets indicate that the mean framework composition ($Q_{97}F_0L_3$) of the sample is quartz-dominated and primarily detrital, although diagenetic imprints, mostly quartz cementation, quartz overgrowth, and other authigenic precipitates, are present. Evidenced by the predomination of monocrystalline quartz grains (99.10%) over the polycrystalline type (0.90%), the dominance of non-undulatory extinction (72.50%), and noticeable euhedral crystals, the compositional framework of the studied quartzose reflects a predominant plutonic provenance with some metamorphic inputs. The possibility of significant sediment reworking is ruled out based on short to moderate transport distance (~100 km) interpreted from the interplay of textural parameters, depositional model, and paleogeography. A humid paleoclimate alongside its associated rigorous chemical weathering is constrained as the dominant control in the formation of the Upper Sarir quartzose sandstone from a dominant craton interior provenance. These conditions probably produced other early Cretaceous arenitic sandstones in other reaches of North Gondwanaland.

1. Introduction

The complex interplay of provenance (e.g., Caracciolo, 2020; Akinlotan et al., 2021), tectonic (e.g., Lorentzen et al., 2019), the interaction of paleoclimate, relief, and sedimentation rate (e.g., Potter, 1978; Suttner et al., 1981; Basu, 1985; Avigad et al., 2005), sediment recycling (e.g., Pettijohn et al., 1987; Johnson et al., 2018; Dott Jr, 2003; Konstantinou et al., 2014), and diagenetic disintegration of incompetent framework components (e.g., Mcbride, 1985; Wahab, 1998; Garzanti, 2017) are the significant factors hitherto identified to be responsible for generating quartz-rich sediments. Globally, 80% of the sedimentary inputs in siliciclastic systems are reportedly produced through sediment reworking (e.g., Cox and Lowe, 1995). However, the general rarity of quartzose/quartzarenite in modern geologic settings somewhat negates the traditional assertion that sedimentary rocks increase in mineralogical maturity with longer transport distance (see Garzanti, 2017). Thus, the current understanding of the formational process(es) of non-diagenetic first-cycle quartz sandstones is still unclear.

Previous studies on the petrogenesis of non-recycled quartz-rich sandstones were based on datasets from northwestern and southeastern USA Holocene sediments (Suttner et al., 1981), early Cambrian Vangas (Norway) and Hardeberga (Sweden) formations (Lorentzen et al., 2018, 2019), early Cretaceous non-marine Wealden Sandstones of the Weald Sub-basin in northwestern Europe (Akinlotan et al., 2021), the Cambro-Ordovician sediments from Pan African terranes (Avigad et al., 2003, 2005), and the Midcontinent Region, USA (Konstantinou et al., 2014). The general paucity of quartz-rich sandstones and the distinction of producing paleoenvironments within different geologic eras necessitate the need to harness all possible data from different geologic periods and terranes to improve our current understanding.

* Corresponding author.
E-mail addresses: jadepehin@ukm.edu.my, jadepehin@gmail.com (E.J. Adepehin).

https://doi.org/10.1016/j.sedgeo.2021.105982
0037-0738/

The early Cretaceous (~143–102 Ma) marked a critical time in Africa because it witnessed the complete separation of the African plate from South America, giving way to the emergence of the South Atlantic Ocean (Fig. 1). Oceanic-atmosphere simulation by Poulsen et al. (2003) suggested that the rifting and subsequent evolution of the Atlantic gateway somewhat contributed to the Cretaceous Thermal Maximum (CTM). By contrast, the CTM, according to Barron and Washington (1985), was occasioned by an increase in atmospheric CO_2 to an excess of 1000 ppm, which was followed by an increase in temperature (Rothman, 2002; Poulsen et al., 2003). The Cretaceous paleoclimate was generally warmer in contrast to the Tithonian (latest Jurassic) (e.g., Sladen and Batten, 1984). Geologically, this period recorded significant events, which include (i) emergence and rapid diversification of flowering plants, (ii) reduction and subsequent extinction of hitherto widespread gymnosperm groups, and (iii) climatic and eustatic changes that initiated global deposition of continental sediments (Müller et al., 2008) among others. In northern Africa, Asia, and the Arabian Peninsula, part of the widely spread Nubian Sandstone (alongside its numerous equivalents) is evidence, though not exclusively, of this unique geologic period (McKee, 1963).

The Nubian Sandstone (early Cretaceous) in the Sirte Basin, Libya (Fig. 2) is subdivided into five lithogroups: Basal Formation, Faragh Formation, Calanscio Formation, Cocolith Formations, and the Sarir Group (El-Hawat, 1992). The latter is generally a subcropped unit segmented into the Lower Sarir Sandstone, Sarir Shale/Claystone, and the Upper Sarir Sandstone formations (Figs. 2D, 3), which is mainly arenitic and the focus of the current research. The subsequent avoidance of the term "Nubian Sandstone" in referring to the studied successions (Upper Sarir Sandstone Formation) in this study is due to its general loose usage (see McKee, 1963; Pomeyrol, 1968; Hassan, 1971; Klitzsch, 1990; El-Hawat, 1992; Morton et al., 2011; Abdel-Fattah, 2021), which has resulted in stratigraphic confusion. Owing to its usefulness as carrier beds, the subsurface sedimentology (Selley, 1968), sedimentary facies (e.g., El-Hawat, 1992; Weihe et al., 2008), petrography (e.g., Alkhazmi, 1988), reservoir quality (e.g., Ambrose, 2000), and pore modification mechanisms (e.g., Ceriani et al., 2002; Ahfaf et al., 2021) of these sandstones have been previously studied. However, very little is documented about its provenance and petrogenesis.

This paper integrates petrographic, sedimentological, and mineralogical proxies to construe provenance and reconstruct paleoprocesses that produced early Cretaceous non-marine first-cycle quartzose, using the Upper Sarir Sandstone Formation, Sirte Basin, as an example. Detailed petrographic and mineralogical interpretations of forty core plugs obtained from the producing interval of the sandstone across three exploration wells in the eastern Sirte Basin were integrated with delineated gamma-ray electrofacies to achieve this objective. Thus, in addition to improving our current understanding of the sedimentological processes that produced non-diagenetic quartzose in the early Cretaceous, this contribution also provides correlatable data for other non-marine quartzose in similar geologic terrains.

2. Regional geological setting and study location

Consequent to the Permian (~299–255 Ma) formation of the Pangea, its Gondwanaland components (South America, Africa, Arabia, Madagascar, Sri Lanka, India, Antarctica, and Australia) migrated slowly toward the northern hemisphere. The North Africa crustal block crossed the equator in the Triassic, and Pangea began to fragment simultaneously (Abdelsalam et al., 2002; Kröner and Stern, 2004; Abadi et al., 2008; Hallett and Clark-Lowes, 2016), although the crustal split was not completed until the early Cretaceous (Fig. 1). At this time, the continental margin of northern Africa was characterized by extension, and crustal thinning, and rifting was mainly along the eastern border of the Africa plate and the southern border of the Arabian plate (Fig. 2A).

The Sirte Basin represents a continentally rifted triple-junction along Africa's northern margin (Fig. 2B, C). It opens to the Mediterranean Sea in the north, where the Gulf of Sirte directly flanks it. Eastwards, the basin is contiguous to the Suluq Low and Cyrenaica Shelf, while its western margin is drawn against the Western Shelf (Fig. 2B). In the south and southeast, the basin's boundaries are pinched at the contact of the Precambrian–Paleozoic along the Nubian Uplift and its northeast-oriented extension referred to as the Southern Shelf.

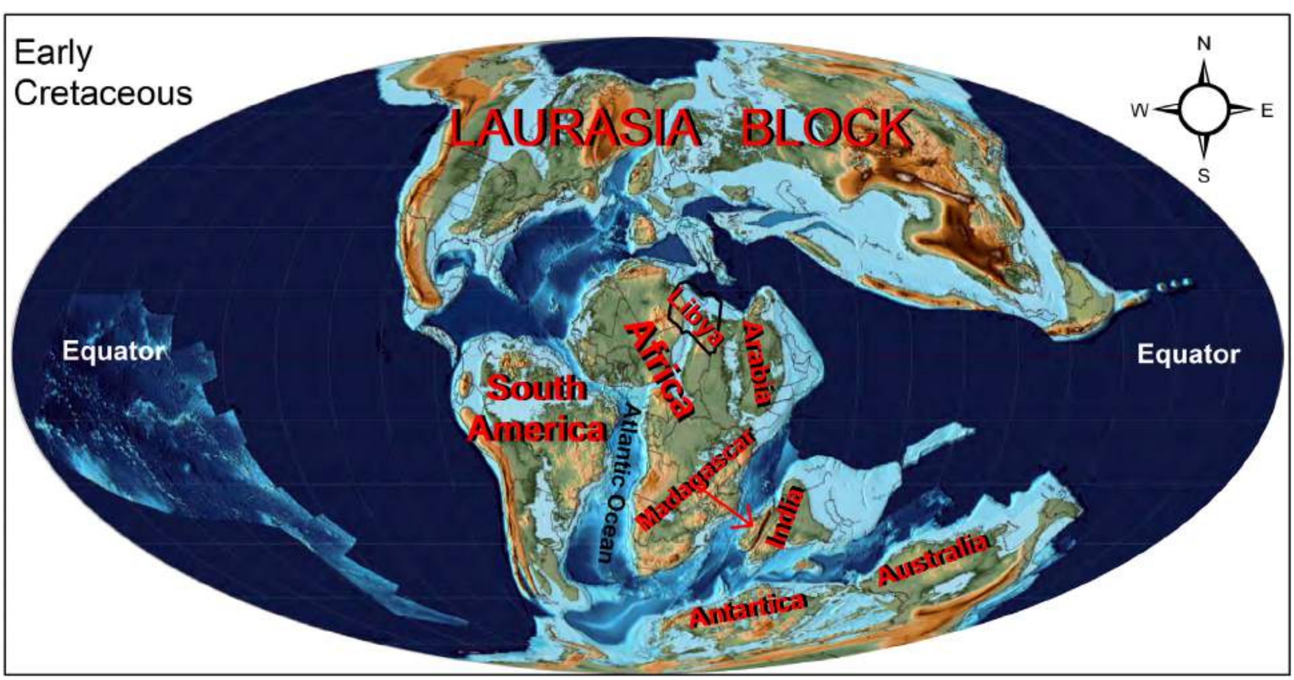

Fig. 1. Early Cretaceous (Late Albian) map of Pangea showing Libya in the Northern Gondwana and visible separation of the African block from its South American counterpart by the Atlantic Ocean.
(After Scotese (2014).)

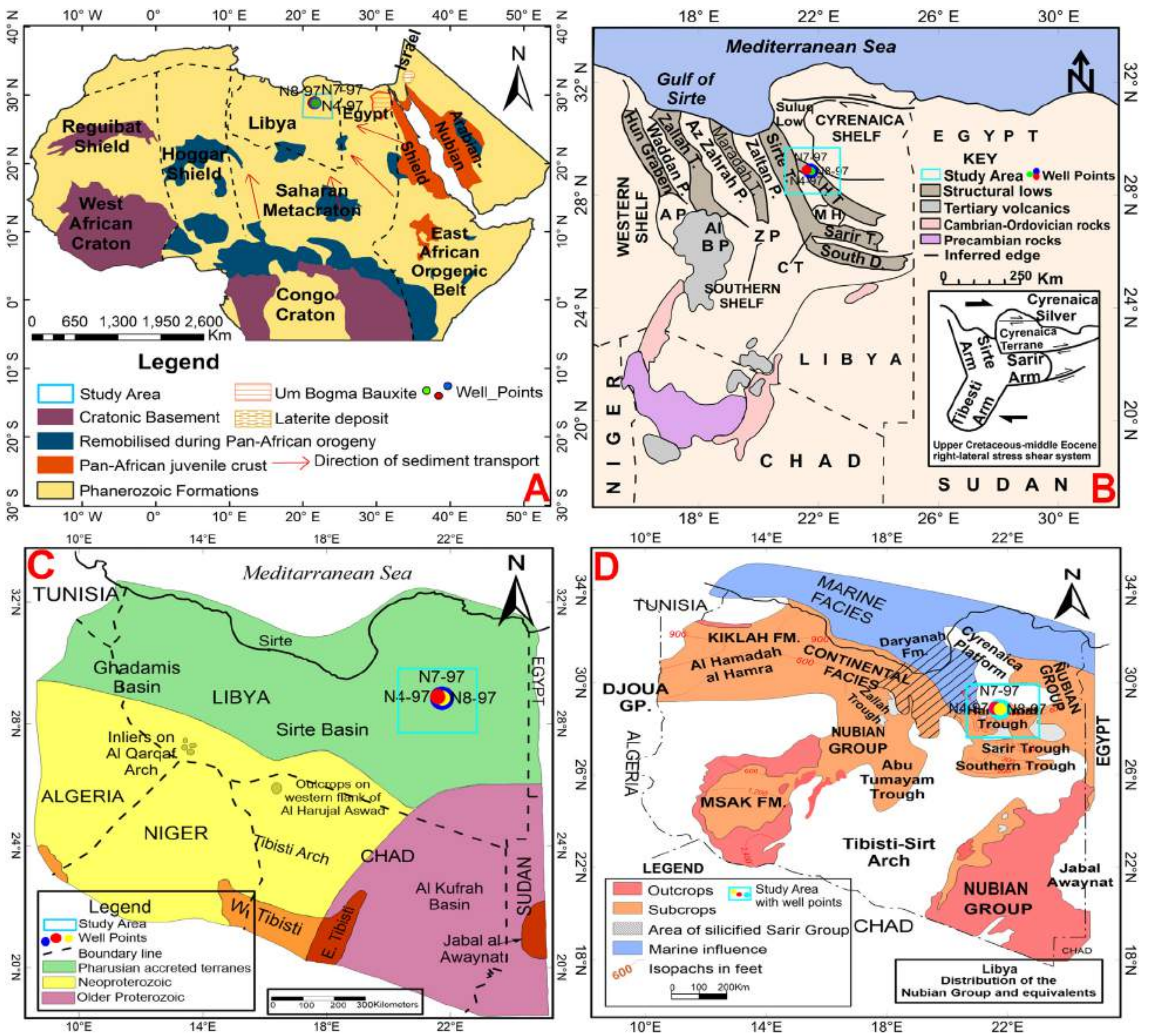

Fig. 2. The study area in northern Gondwana: (A) Map of Africa showing important cratons, Libya, and the primary direction of sediment paleotransport (modified from Meinhold et al., 2011), (B) geological setting of the Sirte Basin showing the triple junction as inset (Ambrose, 2000; Ahlbrandt, 2001), (C) relationship between Sirte Basin and other contiguous basins in northern Libya, (D) basinal distribution of the Nubian Sandstones (including the Upper Sarir Sandstone Formation) and other equivalents showing the study area to be predominantly characterized by subcropped facies (Hallett and Clark-Lowes, 2016).

The structural elements of the basin constituted major sedimentation controls (Fig. 2B–D). Sedimentation in the early Paleozoic was mainly influenced by the NNW and SSE Tibesti-Tripoli Arch (Hallett, 2002; Hallett and Clark-Lowes, 2016). Post-Hercynian orogeny, the Tibesti-Tripoli arch was overprinted by the NNE–SSW oriented Tibesti-Sirte Arch. The evolution of the arch ranged from the Permian through the mid-Cretaceous, and most of the Paleozoic records were concurrently eroded, leading to extensive and widespread deposition of the Upper Sarir Sandstone Formation and its numerous continental lateral equivalents over a significant part of Libya (Fig. 2D).

The northerly oriented “Sirte Arm” of the triple junction (Fig. 2B), which failed to develop into the spreading stage, resulted in an NNW–SSE horst and graben system. The early Cretaceous rifting in the basin reflects the eastern–western oriented strike-slip zone, which is the dominant regulator of siliciclastic accumulations in the Sarir Arm or southeastern Sirte Basin (Anketell, 1996; Abadi et al., 2008). In this arm, an amalgamation of the east–west inclined right-lateral divergent wrench and the northerly structural grain occurred around the Messla High. At the same time, the Calanscio and Sarir Troughs became important depositional centers for the Sarir Sandstone (Fig. 2B, D). According to Ambrose (2000), the Messla High was undisturbed throughout the rifting, whereas a thick succession of syn-rift deposits covered the Calanscio High. The structural configuration of the High is still linked with reactivation of faults at the cessation of the syn-rift phase as well as in the Cenomanian post-rift phase.

Most of the depositional sites and sub-basins within the broader Sirte Basin play host to significant hydrocarbons across varying stratigraphic and structural settings. The depositional model of the Sarir Sandstones indicated that the sediments were principally transported by fluvial systems that originated from the southwestern and, to a lesser extent, the northeastern reaches of the basin covering most of the structural elements, except the Ajdabiya Trough, where significant marine incursion has been recorded (Ahlbrandt, 2001). Stratigraphically, regressive early Cretaceous Sarir Group is unconformity-bounded, sitting unconformably on the Hofram Formation and unconformably overlain by the transgressive sediments of the Bahi and Maragh formations (Fig. 3).

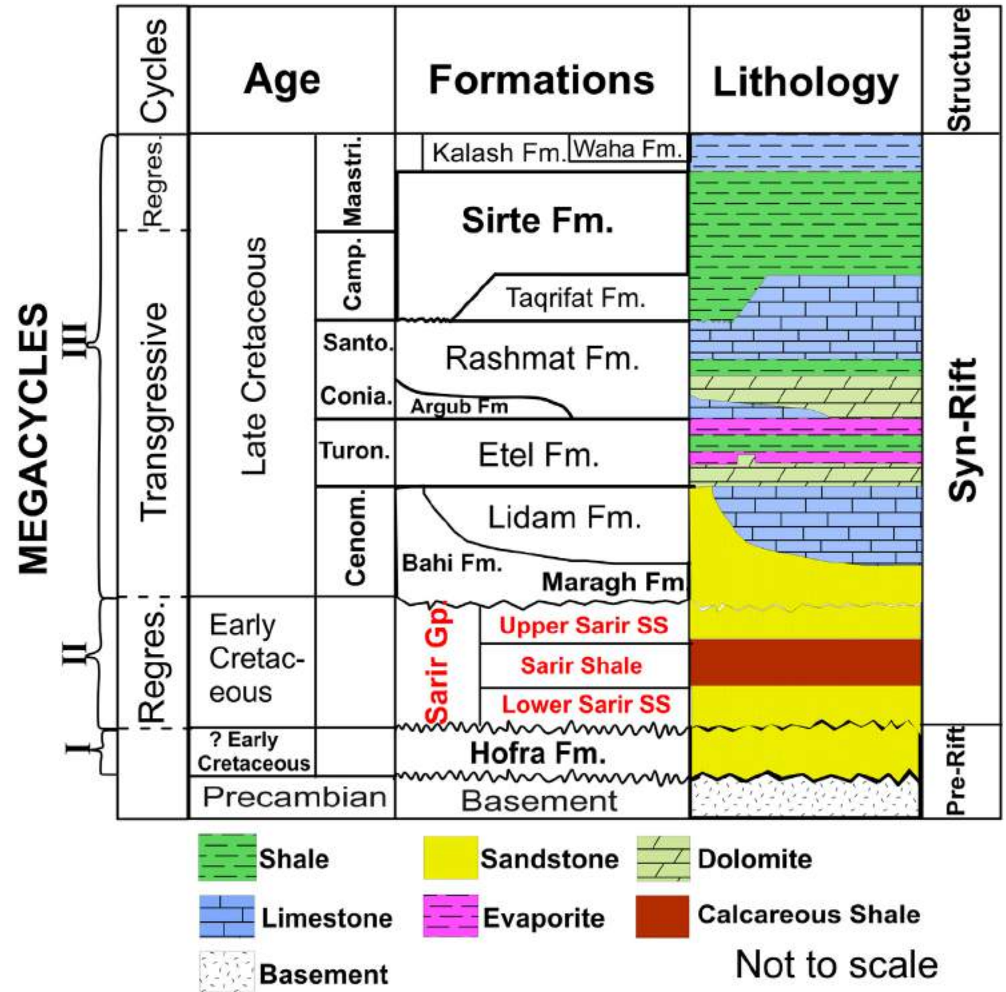

Fig. 3. Pre-rift to syn-rift stratigraphic profile of the study area and corresponding chronostratigraphic cycles of the rock units in the Sirte Basin. (After Haq et al. (1988) and Hallett and Clark-Lowes (2016).)

3. Materials and methods

3.1. Sedimentological description and petrography

The lithological logs of the drilled intervals across the N8-97, N7-97, and N4-97 wells (Fig. 4) were drawn principally with the aid of the recovered core plugs (Fig. 5) and their respective gamma-ray log signatures using a sand–shale cut-off of 90 API (see Ambrose, 2000). The widely used Cant (1992) model for interpreting sedimentary facies and depositional settings from gamma ray signature was adopted to reconstruct the depositional environment of the quartzose sandstone. This model has recently been reviewed (e.g., Nazeer et al., 2016; Radwan, 2021), and it is summarized in Fig. 6. A total of forty core plugs/chips (N8-97: n = 10, N7-97: n = 15, and N4-97: n = 15) of the Upper Sarir Sandstone Formation obtained from the Sarir Field in the Eastern Sirte Basin were used. These plugs were obtained within the depth intervals of 12,470.7–12,539.5 (thickness of 68.8) ft (~3801.1–3822.0 m, thickness ~20.9 m), 12,489.6–12,540.7 (thickness of 51.1) ft (~3806.8–3822.4 m, thickness 15.6 m), and 12,500.7–12,556.6 thickness of 55.9 ft (~3810.2–3827.3 m, thickness 17.1 m), respectively (Fig. 5).

The sedimentological description was carried out on the core chips using a Meiji EMZ 130404 binocular microscope and grain-size comparator to determine textural parameters, such as grain sizes, shapes, colors (using standard color charts), and sorting (Ola and Adepehin, 2017). Prepared thin section slides were petrographically examined using the Leica DM 4500 P microscope. Relevant publications were used as guides for mineral identification (e.g., Mackenzie and Guilford, 1986; Adepehin et al., 2019a, 2019b, 2019c, 2020). Three hundred points were manually counted on each slide using the Gazzi–Dickinson method to aid further interpretation (Dickinson, 1970). To reduce possible biases from point-counting, only an author studied the microscopic slides (see Augustsson, 2021). Acquired petrographic datasets were treated based on the McBride (1963) and Garzanti (2016) schemes to classify the samples. In the former, the lithic vertex is the summation of other rock fragments, carbonate, and chert grains, whereas the point counted quartz, quartzite, and chert were summated to yield the values in the quartz vertex in the latter. The Dickinson and Suczek (1979) ternary plots for treating petrographic datasets to enhance provenance interpretation were adopted.

3.2. Scanning electron microscopy (SEM)

Standard laboratory procedures were adopted to prepare 21 representative samples (same samples used for XRD) of the core plugs (Figs. 4, 5), and their micro-textural parameters were analyzed using variable pressure scanning electron microscopy with energy dispersive x-ray (EDX) spectroscopy. The method described by Adepehin et al. (2019a, 2019b, 2019c, 2020) was adopted. A 1 cm^3 slice of each sample was placed in 4% glutaraldehyde at a temperature of 4 °C for about 14–20 h. After that, the sample was washed for 4 to 10 min with 0.1 M sodium cocodylate buffer. Post fixation of washed samples in 1% osmium tetroxide for 2 h at 4 °C was done, and rewashing with 0.1 M sodium cocodylate buffer

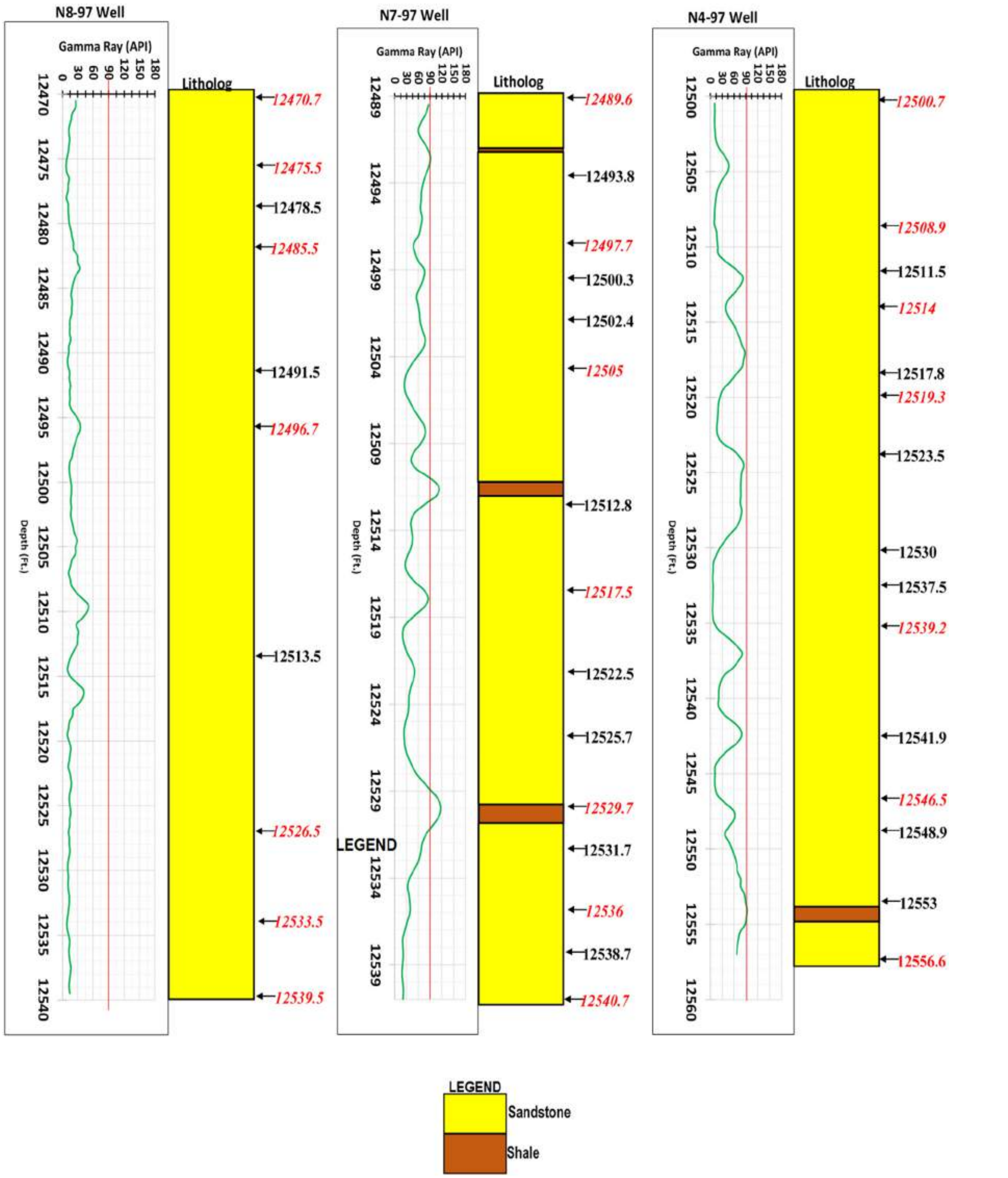

Fig. 4. Lithologs showing the cored stratigraphic intervals and sampling points of the Upper Sarir Sandstone Formation in the three wells used for this study. Note that the formation is essentially sandy and that a generous gamma-ray cut-off of 90API was used in differentiating sandstone and the shaly sandstone in logs.

for three changes of 10 min each was repeated. The rewashed sample was dehydrated using a series of acetone with 35–100% for three recurrent changes. A critical dryer was subsequently used to critically dry the samples for about 30 min. The dried rock slice was stub-fitted and coated with gold in the sputter coater before viewing in VPSEM. The percentage elemental composition and surface elemental mapping were achieved on the samples with the aid of the EDX machine.

3.3. X-ray diffraction analysis

Seven representative samples selected from each of the studied wells (N8-97, N7-97, and N4-97) were subjected to x-ray diffraction (XRD) analysis (Fig. 4). XRD analyzes geological samples by their crystal structure and comparing them with known mineral databases. In this study, XRD analysis and interpretation were executed at the XRD

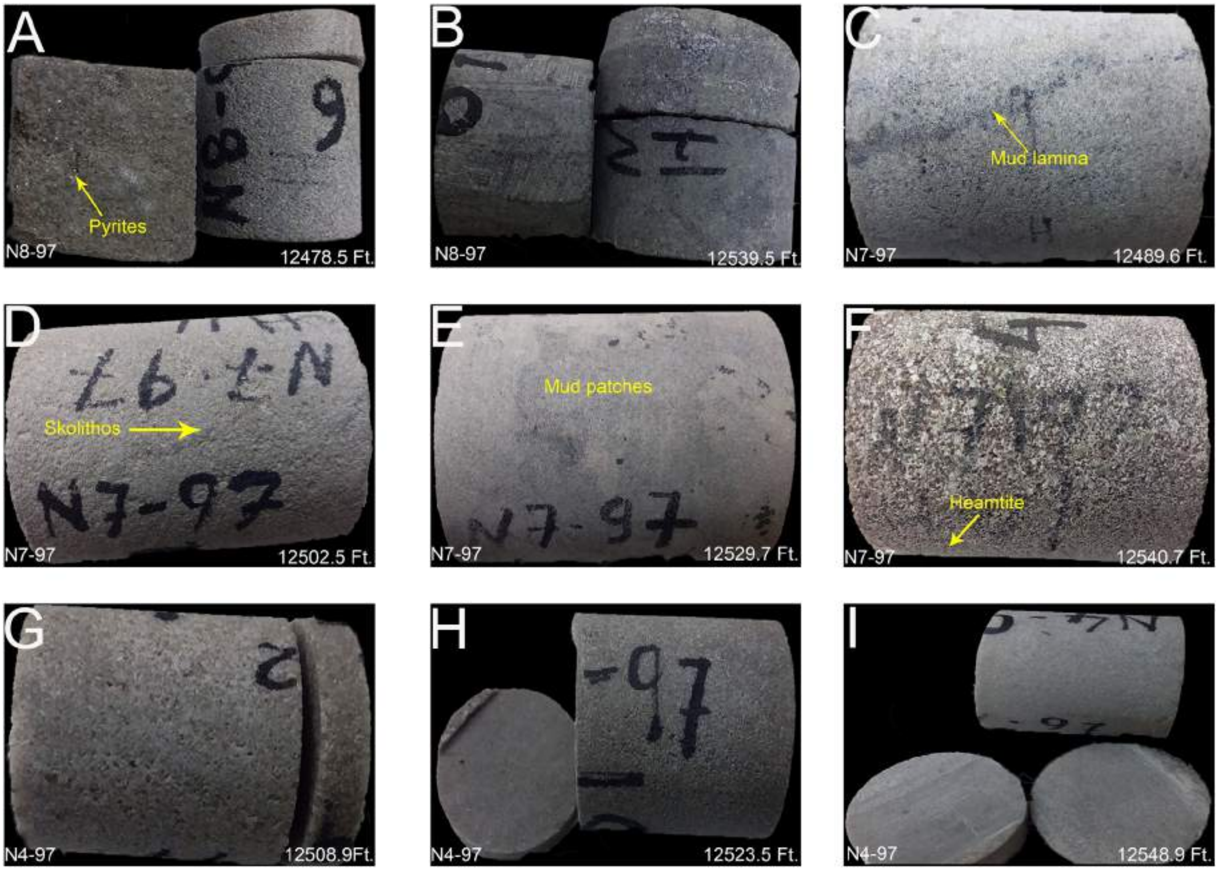

Fig. 5. Representative core chips and plugs of the Upper Sarir Sandstone Formation used for this research. (A) Brownish arenaceous coarse to medium grained sandstone, (B) darkish-gray argillaceous dominantly fine-grained sandstone, (C) dark mud streaks in a quartz-rich fine sandstone, (D) light brownish fine-grained sandstone, (E) dominantly grayish fine sandstone, (F) variegated coarse to medium sandstone, (G) brownish medium-grained sandstone, (H) light brown fine-grained sandstone, (I) grayish to dirty white fine-grained sandstone. (For interpretation of the references to color in this figure legend, the reader is referred to the web version of this article.)

laboratory of the Centre for Research and Instrumentation, the National University of Malaysia, using a standard laboratory method for sample preparation and consequent mineral identification (Brindley and Brown, 1980; Moore and Reynolds Jr, 1997). The Bruker AXS diffractometer (D8 Advance, Germany) with CuKα radiation operating at 40 kV and 40 mA at a step size of 0.025°/step was utilized. Gently powdered core samples were loaded into the sample holder and mounted in the cavity mount of the diffractometer for analysis at an angular range of 5–65°2θ. Obtained XRD data was converted to RAW files using the Kourkoumelis (2013) PowDLLConverter software, after which peak indexation, mineral identification, and background stripping were made with the X'Pert HighScore Plus software. The samples' relative mineral proportions were semi-quantitatively estimated using area ratios of their distinctive peaks with quartz as an internal standard. Estimated mineral percentages were used for mineral relative abundances only and not absolute values. The agate mortar and pestle used for disaggregating samples were washed and oven-dried after crushing each sample to prevent sample contamination.

4. Results and interpretation

4.1. Sample description, petrography, and mineralogy

The core plugs and chips of the Upper Sarir Sandstone Formation (Fig. 5) are indurated and dominantly arenaceous, with increasing argillaceous components in the N7-97 and N4-97 wells (Fig. 2; Appendix 1). The studied cored interval in the N8-97 well comprises brownish-to-grayish-to-whitish, moderately well-sorted to very well sorted, angular to rounded medium fine-grained sandstones (Fig. 5). Sedimentary structures were generally indiscernible (Fig. 5A, B). Some unique features of the plugs are the rare occurrences of *Skolithos* burrows, clay patches, and hematite coating. Silicious cement and ferruginous coating are commonly present and become increasingly prevalent downhole. Unlike the N8-97 well, assorted coloration is less prevalent in the core plugs of the N7-97 well (Fig. 5C–F). It is dominantly grayish, very well-sorted to moderately well-sorted, subangular to rounded, and medium to fine-grained. Sedimentary structures are generally unnoticeable due to the relative size of the samples (Fig. 5C–F), but small-scale mud lamina and mud patches are evident in some of the studied core plugs (Fig. 5C, F). The cored successions in the N4-97 well are characterized by variegated grayish to whitish coloration (Fig. 5G–I), and it is texturally very well-sorted to moderately well-sorted, rounded to subrounded, and medium to fine-grained.

Petrographically, the studied samples of the Upper Sarir Sandstones Formation are classified as quartz-rich sandstone, evidenced by its texturally sub-mature to mature signature (Figs. 7–9; Appendix 1) and mineralogical maturity indices (Figs. 5, 10). An estimated 97.5% and 87.5% of the samples cluster within the quartzose (Fig. 7A) and quartzarenite (Fig. 7B) fields of the triangular interpretative models. The samples are generally moderately well-sorted to well-sorted and angular to subangular quartz grains in thin sections (Fig. 8). The thin sections are essentially devoid of feldspars, and orthoclase generally dominated plagioclase grains when present (Figs. 7, 8). The compositional framework of the samples is dominated by monocrystalline quartz grains, which range in composition from 69.33% (12,536 ft or ~3820.1 m) to 87.67% (12,525.7 ft or ~3817.8), with the upper and lower values occurring in the N7-97 well. Modal analysis indicated that ~52.5% of the samples are devoid of polycrystalline quartz (see

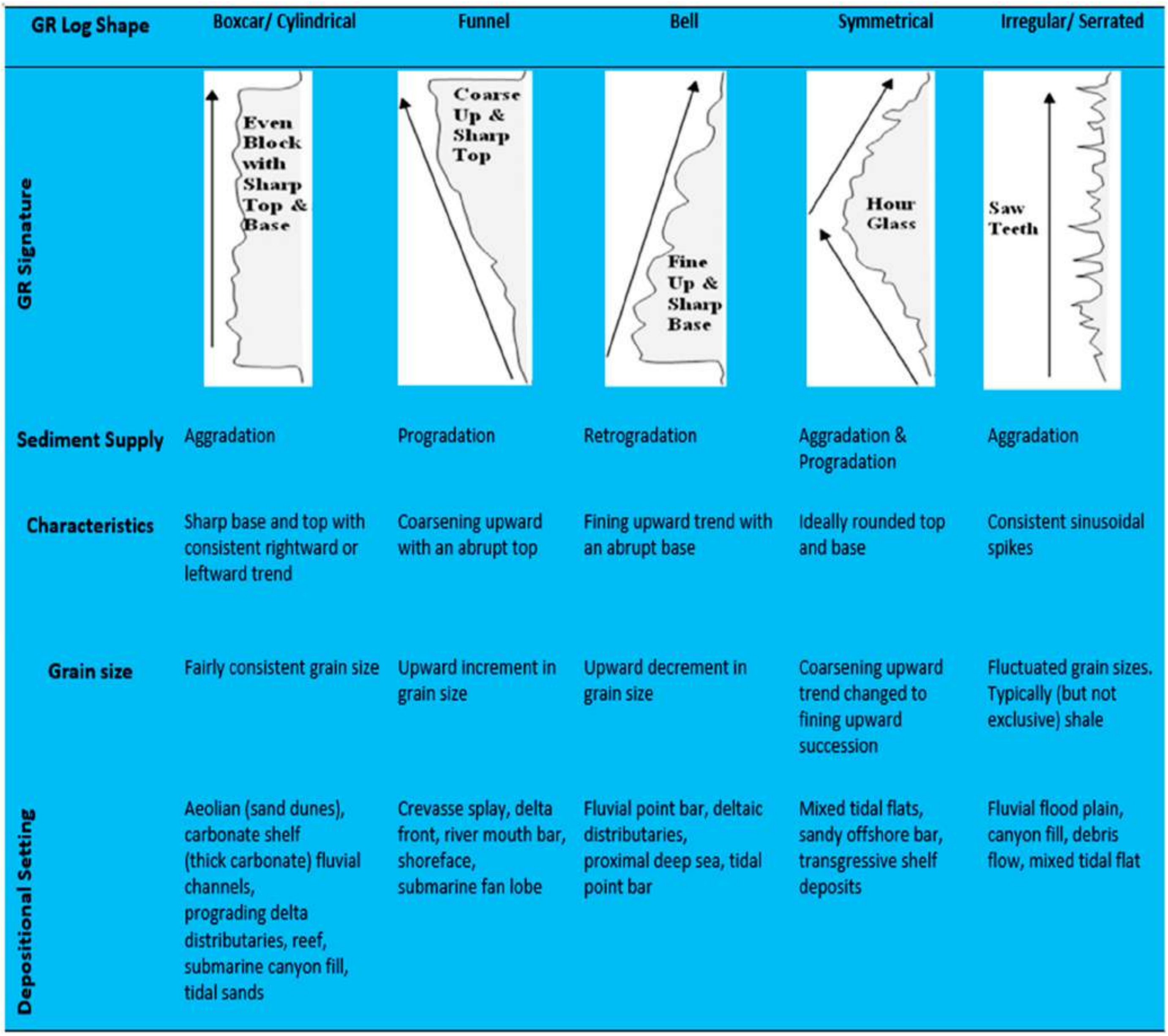

Fig. 6. Prominent electrofacies associate with gamma-ray log motifs.
(After Cant (1992), Nazeer et al. (2016), and Radwan (2021).)

Fig. 8F), whereas the highest occurrence (5.33%) of polycrystalline quartz was observed at a depth of 12,548.9 ft (~3825.2 m) in the N4-97 well (see Appendix 1). Quartz grains generally show distinctive euhedral form (see Fig. 9D–F), and they are characterized by non-undulating (72.50% of the samples) and undulating extinction, with the former dominating the latter. Rock fragments are mainly igneous, metamorphic, and metasediments (shaly). The average quartz–feldspar–lithic composition of the Upper Sarir Sandstone Formation based on the studied interval is $Q_{97}F_0L_3$ (Fig. 7). Grain-to-grain relationships are largely tangential and long contact types (Fig. 8), and grains are commonly tightly packed (Fig. 8A–E), resulting in a significant reduction in intergranular pores. Matrices are rare and are generally muddy/clayey when present (Figs. 8E, F, 9E).

Representative diffractograms of the studied sandstones further support the presented petrographic data (Fig. 10) that quartz is the dominant mineral (Fig. 10A), constituting an estimated mineralogical composition of 79.70 at 12539.5 ft (~3822.0 m) in well N8-98 to 95.40% at 12505 ft (~3811.5 m) in well N7-98 (Figs. 7, 8). Calcite formed less than 6.00% of the total minerals in the studied samples, while siderite ranged from 0.0 to 3.3%. Other minerals, such as K-feldspar, albite, hematite, rutile, pyrite, glauconite, anatase, siderite, paragonite, illite/muscovite, cronstedtite, nacrite, kaolinite, chamosite, and chlorite erratically occur in the samples, but their presence is evident downhole (Fig. 10).

4.2. Detrital versus diagenetic imprints

Notwithstanding the conspicuous detrital (chemically unaltered) nature of the framework grains in the studied sandstone samples (Figs. 8, 9, Appendix 1), notable post-depositional alteration of non-framework grain components is evident (e.g., Figs. 5, 8F, G, H). Visible post-depositional fractures are evident in some quartz grains (Fig. 8B, D, F) due to the compactional stress exerted by overlying late Mesozoic to Tertiary syn-rift and post-rift beds (see Fig. 3). In addition to the significant reduction of porosity by the tight packing of framework grains through compaction (Fig. 8A, B), intergranular pores are significantly

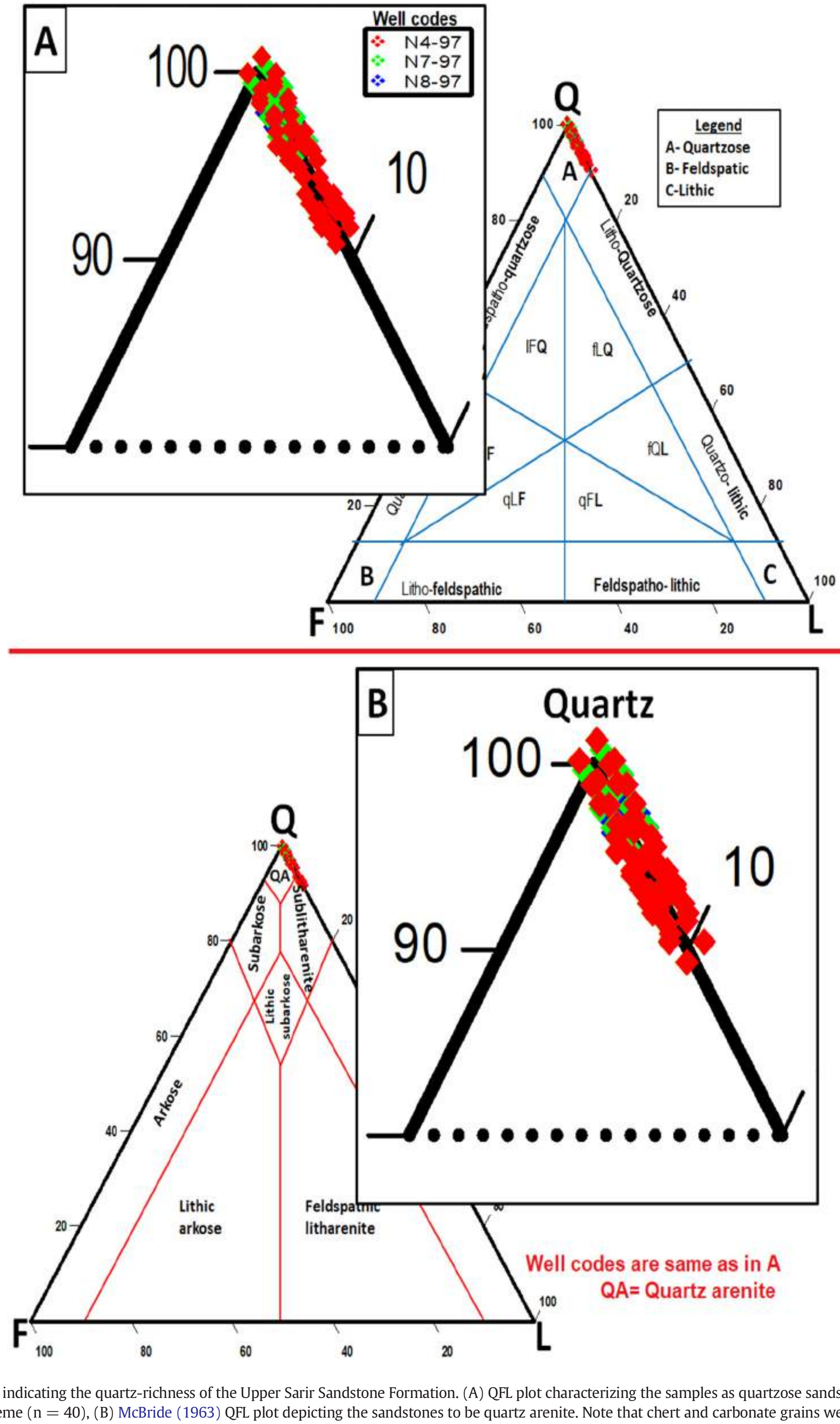

Fig. 7. Petrographic plots indicating the quartz-richness of the Upper Sarir Sandstone Formation. (A) QFL plot characterizing the samples as quartzose sandstone following the Garzanti (2016) classification scheme (n = 40), (B) McBride (1963) QFL plot depicting the sandstones to be quartz arenite. Note that chert and carbonate grains were treated as lithics and are thus inclusive in the "L" Vertex in Fig. A; meanwhile, chert and quartzite grains were counted as quartz and thus, these grains are included in the "A" pole of Fig. B (n = 40).

occluded by quartz cement and overgrowth (Fig. 8A–D, F), the latter being the most dominant pore cement types (see Fig. 8A–D). Mud, authigenic chlorite, and sericite occur as pore-filling and rarely as grain coating materials (Fig. 8F–H). Though rare, precipitated euhedral quartz crystallites and micro quartz are visible as pore-filling materials within the framework (Fig. 9A–C, H, I).

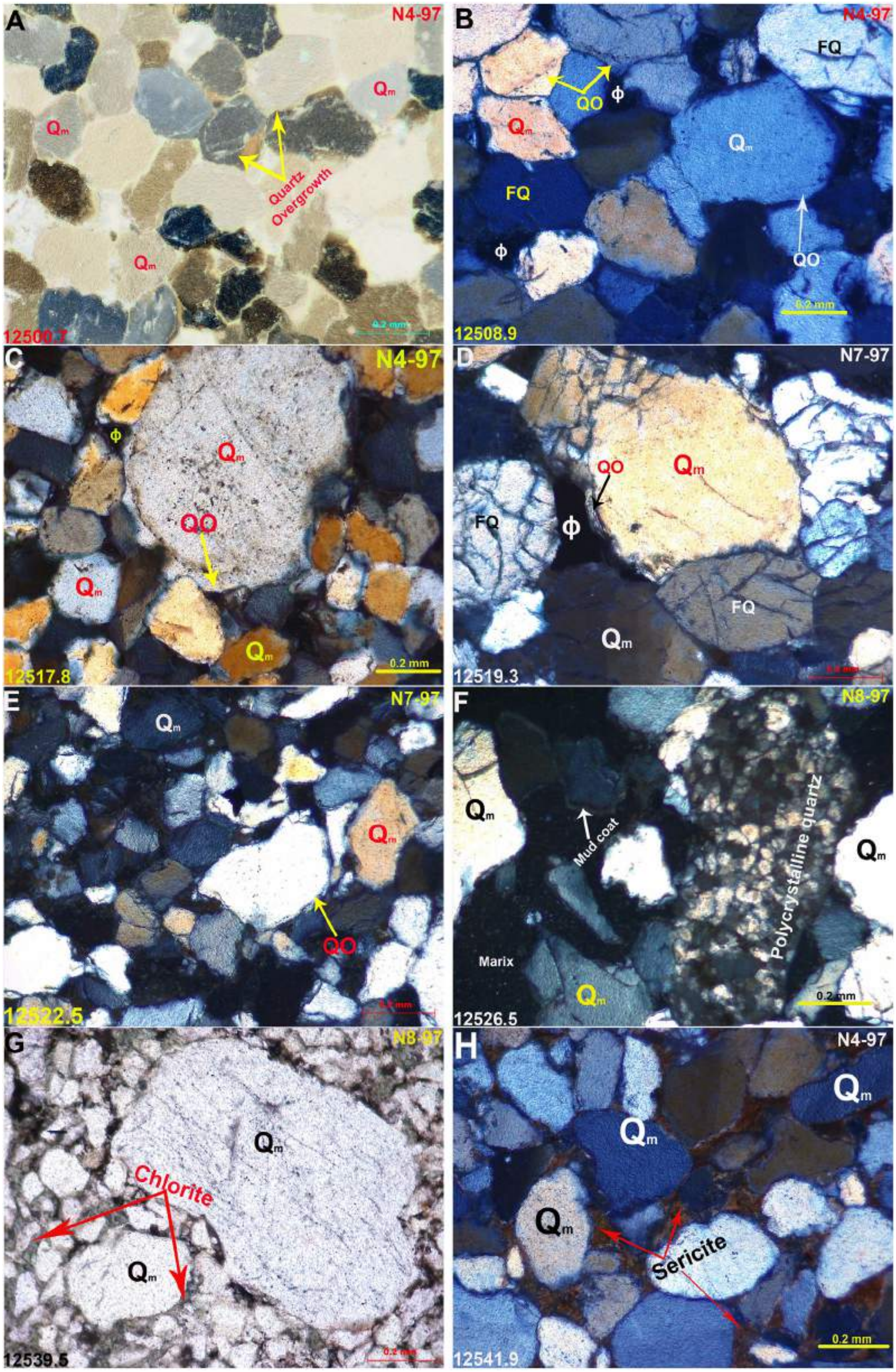

Fig. 8. Representative thin section microphotographs of the Upper Sarir Sandstone Formation. (A) Well-sorted, dominantly-subrounded, matrix-deficient, and grain-supported fine-grained monocrystalline quartz sandstone showing quartz overgrowth, (B) moderately well-sorted, dominantly-subangular, medium-coarse grained monocrystalline quartz sandstone showing intergranular pores and overgrowth of quartz, (C) very coarse quartz grain embedded in dominantly fine and subrounded monocrystalline detrital quartz, (D) dominantly coarse, subrounded, matrix-devoid, and strained quartz grains in quartz sandstone, (E) subangular, clay matrix-supported, and moderately sorted monocrystalline quartz sandstone, (F) polycrystalline quartz grains immersed in clay-coated and matrix-supported monocrystalline quartz grains framework, (G) coarse quartz grains in dominantly fine and authigenic chlorite-coating quartz sandstone, (H) intergranular sericitic filling in subangular to subrounded coarse-grained. Note that all microphotographs are in xpl, Q_m is monocrystalline quartz, QO is quartz overgrowth, ϕ is intergranular pores. The names and depths of each sample are on the microphotographs.

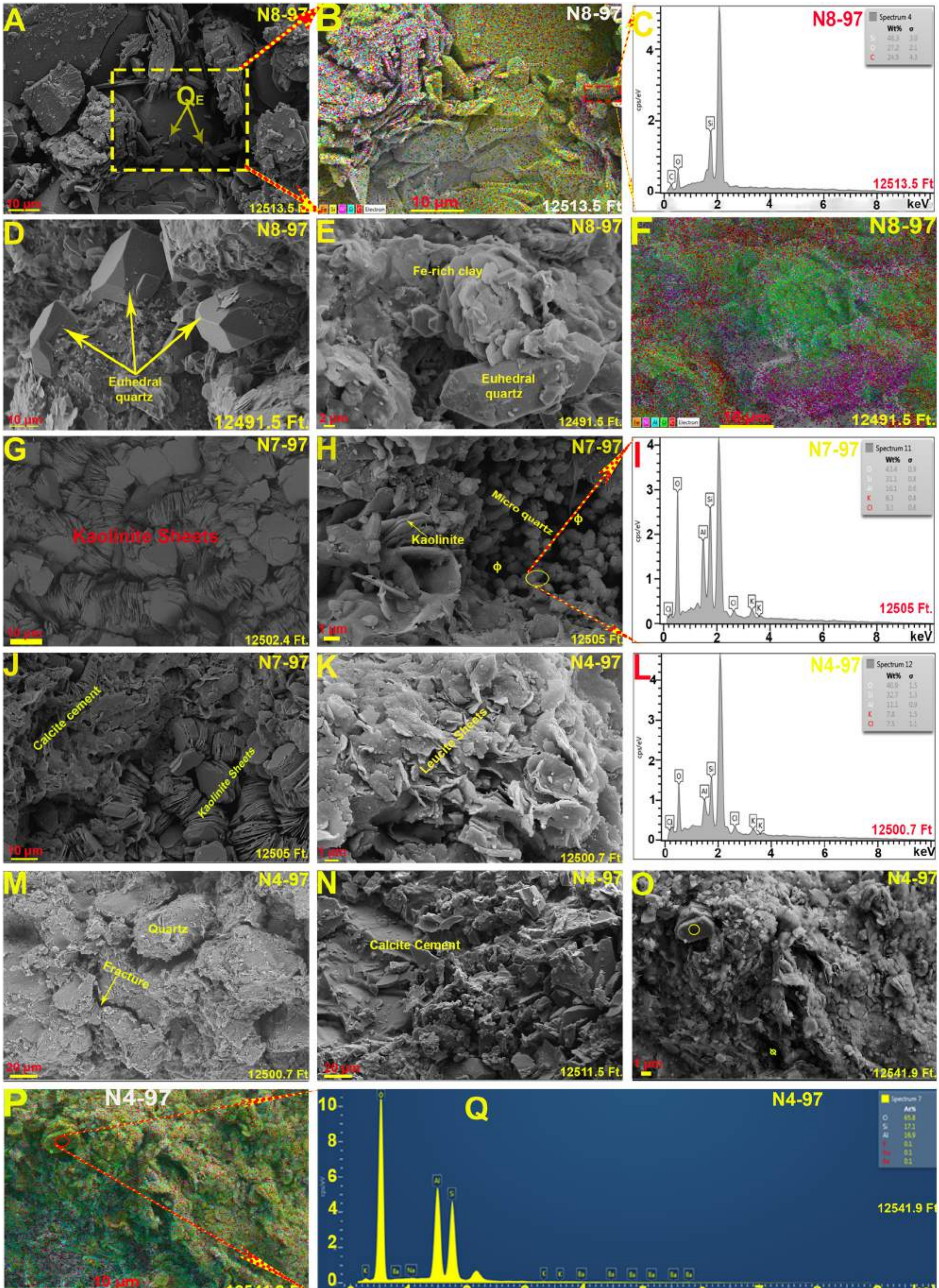
A
N8-97
QE
10 μm
12513.5 Ft
B
N8-97
10 μm
12513.5 Ft
C
N8-97
Spectrum 4
12513.5 Ft
keV
D
N8-97
Euhedral quartz
10 μm
12491.5 Ft.
E
N8-97
Fe-rich clay
Euhedral quartz
2 μm
12491.5 Ft.
F
N8-97
10 μm
12491.5 Ft.
G
N7-97
Kaolinite Sheets
10 μm
12502.4 Ft.
H
N7-97
Micro quartz
Kaolinite
ϕ
1 μm
12505 Ft
I
N7-97
Spectrum 11
12505 Ft.
keV
J
N7-97
Calcite cement
Kaolinite Sheets
10 μm
12505 Ft.
K
N4-97
Leucite Sheets
1 μm
12500.7 Ft
L
N4-97
Spectrum 12
12500.7 Ft
keV
M
N4-97
Quartz
Fracture
20 μm
12500.7 Ft
N
N4-97
Calcite Cement
20 μm
12511.5 Ft.
O
N4-97
1 μm
12541.9 Ft.
P
N4-97
10 μm
12541.9 Ft.
Q
N4-97
12541.9 Ft
keV

Although not visible in thin section, kaolinite sheets in SEM images occur as both detrital and authigenic components (e.g., Fig. 9G–J) and sometimes in close contact with calcitic cement (Fig. 9J). Whereas the authigenic kaolinite occurs within the pore system (9H), most of the observed kaolinitic sheets are non-pore occluded (see Fig. 9G, I, J). This notwithstanding, chlorite is mainly pore-occluding and sometimes grain coating suggesting that its evolution postdated the deposition of the sandstone (Fig. 8G). Sericite occurs very sparingly in the Upper Sarir Sandstone Formation across the studied intervals (e.g., Fig. 8H), but it exerts significant influence on detrital intergranular pores when present. These alongside the common occurrences of intergranular sideritic crystallites (Appendix 1) support diagenetic influence on the non-framework components of the quartz-rich sandstone in the Upper Sarir Sandstone Formation (Figs. 4, 5, 8).

4.3. Subsurface variation of mineralogical, textural, and electrofacies signatures

Notwithstanding the fluvial deposited and quartzose nature of the Upper Sarir Sandstone Formation, significant downhole variation can be observed in the mineralogical and textural signatures of key parameters (see Fig. 10). The calculated quartz composition from the XRD data yielded consistently higher values than the point-counted quartz grains all through the studied interval across the three wells, whereas point-counted monocrystalline quartz is almost equal to the total counted quartz grains (Fig. 11). The observed higher percentage composition in the XRD-measured quartz compared to the point counted grains reflects quartz contributions from diagenetic quartz materials such as overgrowth and intergranular quartz cements (see Figs. 8, 9) that are normally not counted alongside detrital grains in petrographic analysis. Percentage feldspar downhole was generally less than 1% (see Appendix 1), and as such could not be accommodated in Fig. 10B. Although inconsistent, a somewhat inverse relationship is evident between total lithics and matrix composition in Fig. 11, with the upper section (12470–12,480 ft) of the N8-97 well recording the highest variation. The matrix composition in the upper region of the well (12470–12,520 ft) generally exceeds counted lithics, whereas the reverse is the case below 12,525 ft downhole (Fig. 11).

The percentage cement (and replacement) also varies indirectly with the calculated intergranular volume (IGV). Though generally less than 15%, IGV consistently decreases downhole, confirming the joint influences of compaction and cementation processes that are evident in the presented photomicrographs (Figs. 8, 9). Calculated percentage lithic types show that igneous (range 0–100%) and metamorphic (range 0–30%) rock fragments, including mildly metamorphosed shales (≤40%) are the dominant lithic materials, although with inconsistent vertical trends downhole (see Panel C, Fig. 11). Unresolved lithic components plotted as undifferentiated lithics are perhaps metasedimentary rocks, and they constitute about 0 to 30% of total lithics within the studied intervals. Notwithstanding minor variations, the downhole trends in the N7-97 and N4-97 wells within the studied intervals are generally like that of the N8-97 well as discussed above and illustrated in Fig. 11. Stratigraphically, kaolinite dominated the clay types in the Upper Sarir Sandstone Formation between 12,470 and ~12,495 (ft), while the depth beneath 12,525 ft shows notable but intermittent percentage chlorite composition.

The gamma-ray log motifs across the three wells yielded a dominantly saw-tooth pattern (Figs. 6, 12), and slightly fining-up succession with abrupt bases at the lowermost sections of the N8-97 (~12,517–12,540 ft) and N7-97 (~12,530–12,541 ft) wells. On these bases, two electrofacies are distinguished, electrofacies A (retrograded, fining upward fluvial point bar facies) and electrofacies B (aggraded fluvial flood plain facies).

5. Discussion

The chemically unaltered nature of the framework grains evidenced by the general absence of dissolution porosity in the studied samples indicates its quartzose nature was not diagenetically induced (Fig. 8). In addition to the conspicuous dissolution of grains, quartz-rich sandstones produced by authigenic processes usually generate significant diagenetic clay minerals and their derivatives (Eberl, 1984; Millot, 2013; Adepehin, 2019; Adepehin et al., 2020). Thus, the generally low composition of illite (≤1.70%), cronstedtite (≤1.50%), nacrite (≤0.50%), kaolinite (≤9.70%), chamosite (≤5.2%), and chlorite (≤4.3%) across all the samples vis-à-vis the absence of dissolved grains ruled out the possibility of notable clay transformation (Figs. 9, 10), although some forms of neoformation might have taken place. These indicate a pre-depositional to syndepositional quartz-richness for the Upper Sarir Sandstone Formation detritus in the eastern Sirte Basin. Thus, possible pre-depositional and syndepositional controls that produced the quartzose sandstones include (i) provenance and tectonic setting, (ii) paleoclimate and weathering, and (iii) sediment transport history and depositional energy. These are discussed below in the light of the presented datasets.

5.1. Provenance and paleotectonic setting

The low (<4%) joint composition of total feldspar and unstable lithic grains in each sample (Figs. 5, 11) and the converse high quartz grains (>96%) in the sandstones of the Upper Sarir Sandstone Formation classify them as quartzose sandstones or quartzarenite. The general clustering and overlapping of the plotted petrographic data for the analyzed samples in the craton interior field of the QFL and Q_mFL ternary diagrams suggest the sandstones are essentially derivatives of passive platform or continental blocks, with few showing recycled orogenic imprints (Fig. 13A–C). Sedimentologically, this craton-sourced quartzose is interpreted as products of flat-lying intrusive rocks and metamorphosed (gneissic) rocks, perhaps with some inputs from recycled sediments generated from these low-lying platforms (Dickinson, 1985). Thus, the high ratio of monocrystalline quartz to polycrystalline quartz grains, as well as the general preponderance of K-feldspar to plagioclase in the samples, notwithstanding the general rarity of feldspars (Appendix 1), characteristically supports the derivation of the studied quartzose from plutonic basement rocks. The general dearth of smectite (see Figs. 9, 10 Appendix 1), whose presence is known to depict volcanogenic sedimentary inputs (Chamley, 1989), in the samples further supports a predominantly plutonic origin for the sediments.

However, the documented polycrystallinity of some quartz grains (e.g., Fig. 8F) is suggestive of contributions from metamorphic sources. A metamorphosed sediment source is supported by the recorded occurrences of euhedral quartz crystals in the microphotographs of the sandstones (Fig. 9A, D, E, F), which according to Akinlotan et al. (2021) could be indicative of a quartzitic sediment source or its arenitic derivatives. Though with an uncertain stratigraphic position, pre-rift, well-cemented and mineralogically mature quartzites that predate the

Fig. 9. SEM images, EDX plot, and surface elemental mapping of representative quartzose of the Upper Sarir Sandstone Formation. (A) Euhedral small quartz grain surrounded by non-framework matrix and cement, (B) surface mapping of the marked region in (A) indicating Al (clay) dominated the leftward region of the sample whereas Si (quartz) most area, (C) EDX elemental plot of marked area in Fig. 5B showing Si as the dominant mineral, (D) detrital euhedral quartz grains surrounded matrix material within sandstone framework, (E) iron-rich clay flanking a well-formed euhedral quartz grains, (F) surface elemental mapping of Fig. 5F showing significant presence of Fe, O, and Si, (G) sheets of kaolinite grains stacked within sandstone framework, (H) aggregates of microquartz occurring with pore-system, (I) spot EDX plot of Fig. 5H showing high silica and oxygen contents, (J) kaolinite crystals flanking calcite cement within sandstone framework, (K–L) high resolution image of leucite and accompanying EDX plot, (M) stress-induced fracture within sandstone framework, (N) calcite cement, (O) euhedral quartz grains within clay matrix materials, (P–Q) surface elemental map of Fig. 5O and EDX plot.

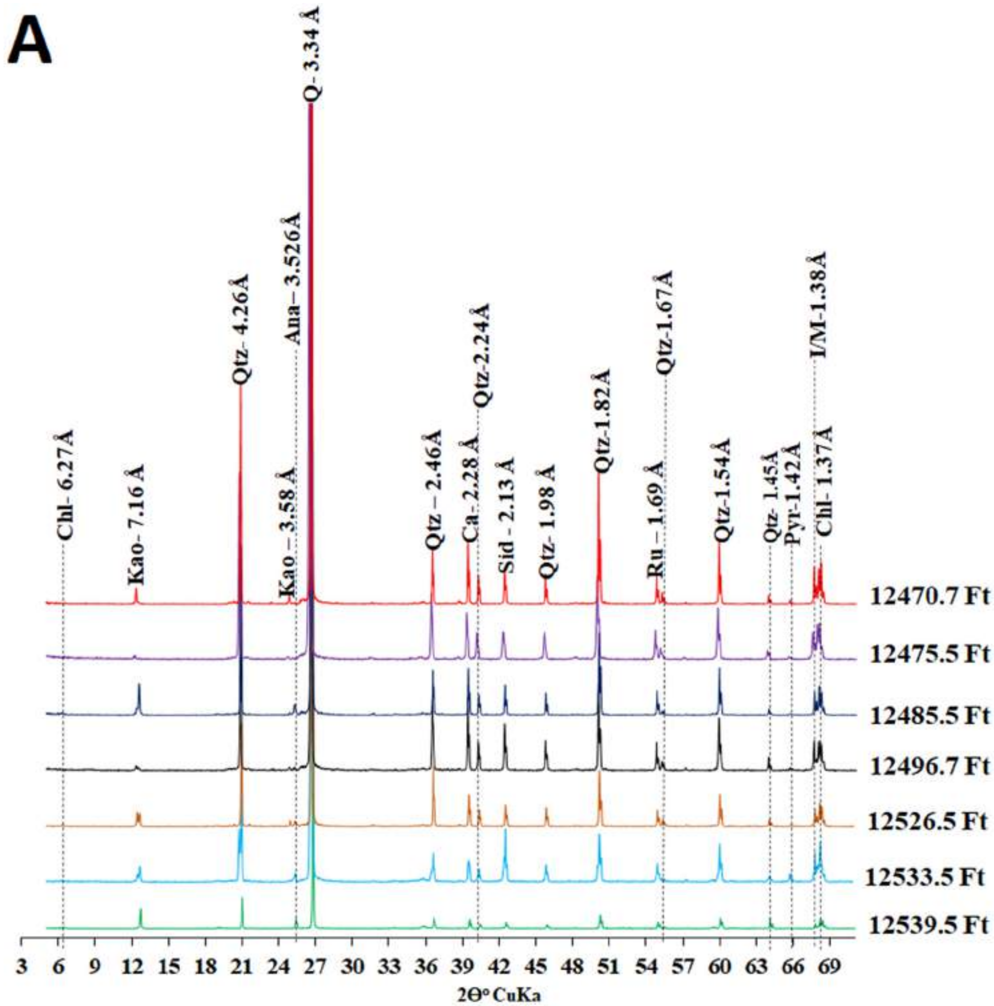

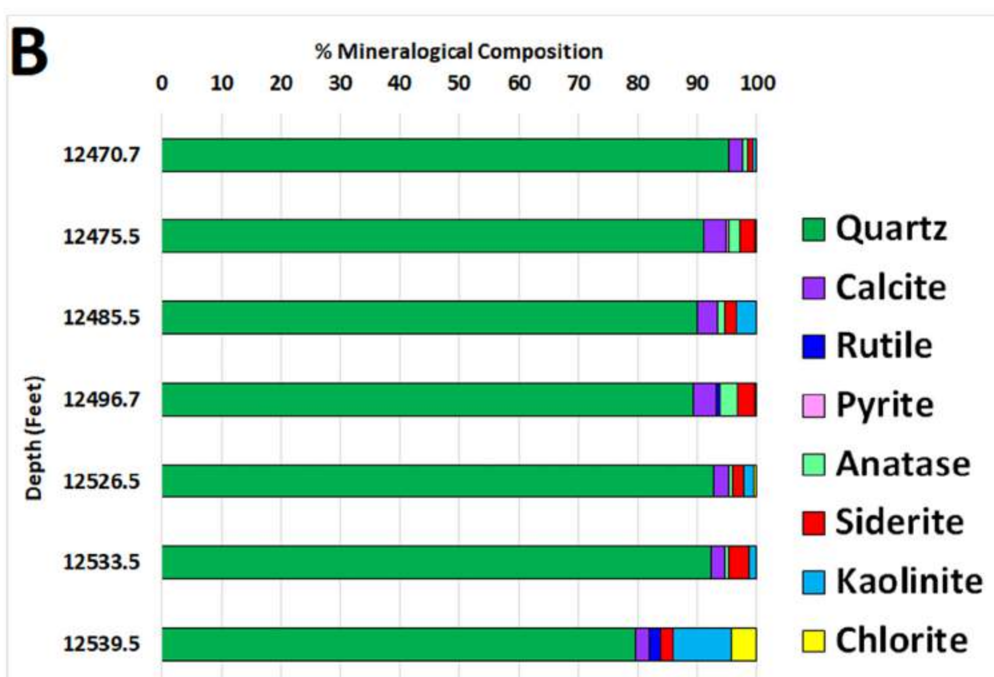

Fig. 10. (A) Stacked XRD diffractograms showing the variation of mineralogical peaks in the N8-97 well. Note the consistent occurrence of kaolinite peaks downhole. Qtz, Chl, Kao, Ana, Ca, Sid, Ru, Pyr, and I/M denote quartz, chlorite, kaolinite, anatase, calcite, siderite, rutile, pyrite, and illite/mica, (B) percentage occurrence of principal mineralogical composition in representative samples of Upper Sarir Sandstone Formation in N8-97 well based on the XRD data presented in A.

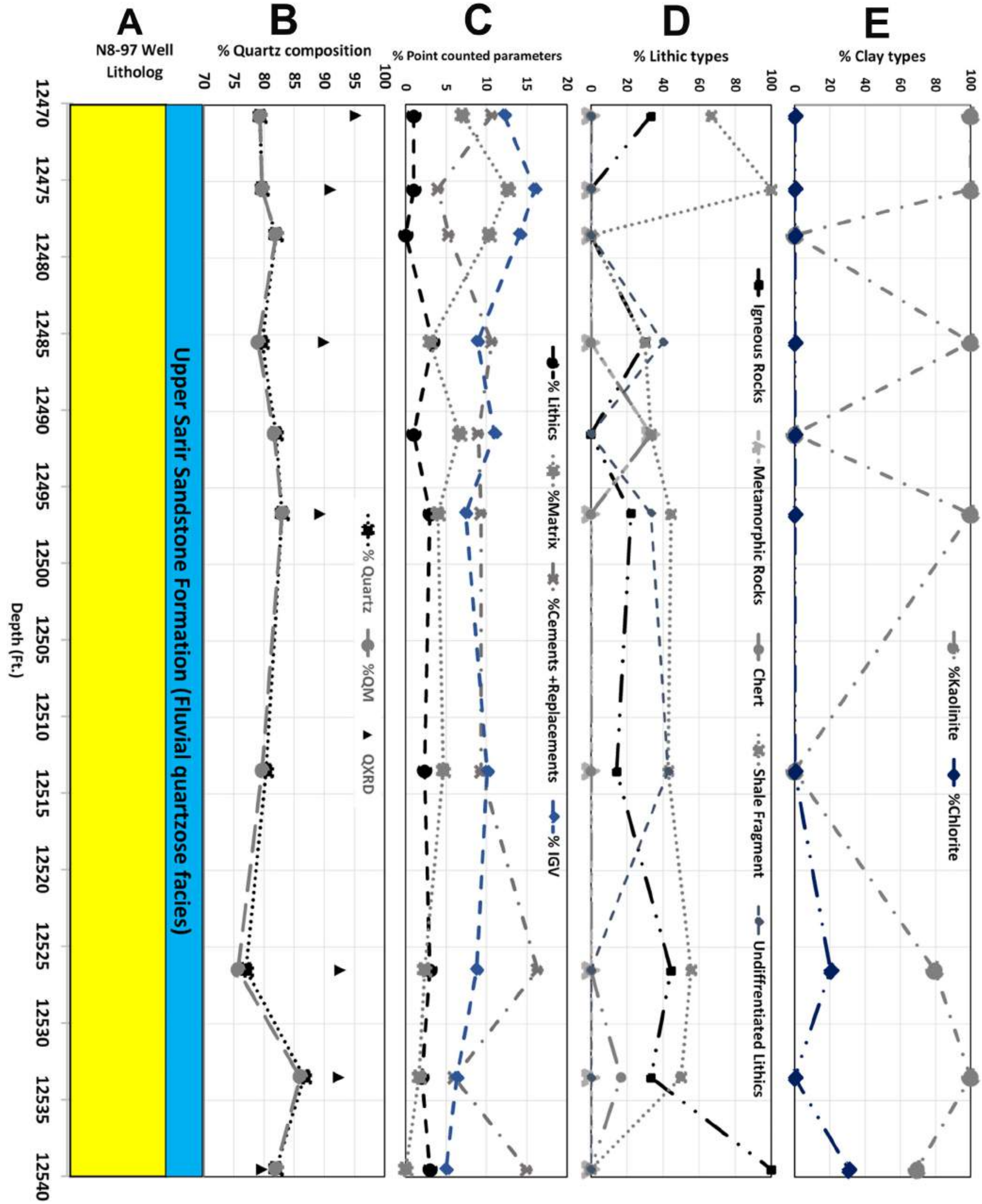

Fig. 11. Downhole correlation of important mineralogical and textural parameters in the Upper Sarir Sandstone Formation based on the studied interval in N8-97 well. (A) Lithological section of the studied interval (B) percentage point counted quartz, monocrystalline quartz, and XRD-determined quartz composition, (C) line graphs showing stratigraphic variation of percentage lithics, matrix, cement with dissolution, and intergranular volume (IGV), (D) downhole occurrences of igneous, metamorphic, metasedimentary (shale), chert and undifferentiated lithics, (E) percentage types showing preponderance of kaolinite, little chlorite and dearth of other clay mineral types.

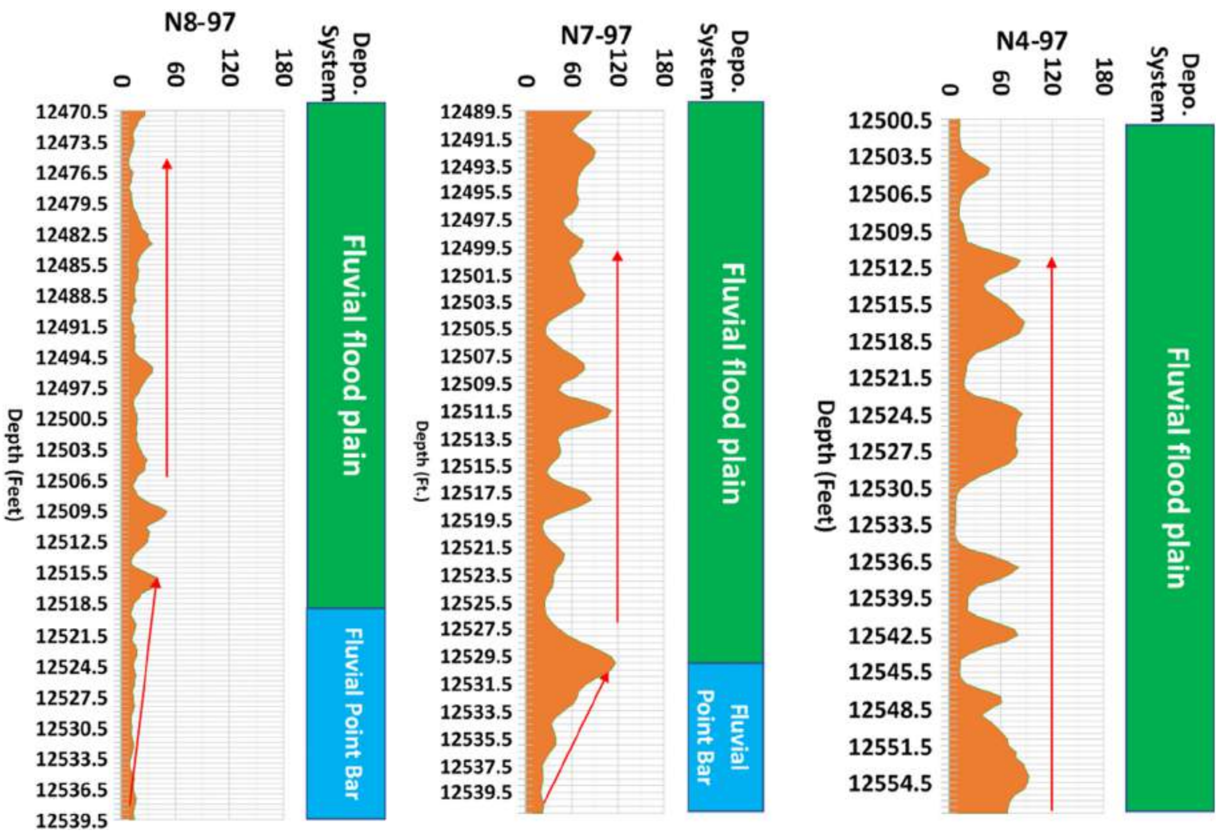

Fig. 12. Interpreted electrofacies for the studied intervals across the three wells based on gamma-ray signature and log patterns.

early Cretaceous unconformity (Fig. 3) have been previously reported in Sarir Field, Eastern Sirte Basin (e.g., Selley, 1997). These quartzites are thought to be the products of intense weathering of arenaceous formations impacted by prolonged uplift of the Tibesti-Sirte arch (Hea, 1971). The usefulness of quartz extinction as a provenance indicator has been debated without a consensus hitherto (e.g., Blatt, 1967; Basu et al., 1975; Basu, 1976). Nevertheless, quartz crystallites with non-undulate extinction are taken to be derivatives of plutonic igneous parent rocks (e.g., Blatt and Christie, 1963; McKosky, 1975). Hence, the display of non-undulatory extinction in an estimated 72.50% of the studied samples gives credence to our interpretation of predominantly plutonic source massifs.

From the paleogeographic point of view (Figs. 2A, 14), the studied detritus could have been partly contributed by the northerly oriented syn-rift sediment inputs from the Arabian–Nubian Shield and pockets of Cambro-Ordovician sandstones that were remobilized during the Pan-African Orogeny (Beauf et al., 1971; Selley, 1972, 1997; Dabbagh and Rogers, 1983; Avigad et al., 2005). However, significantly reworked Cambro-Ordovician Sandstones might not have been transported beyond the reaches of the Saharan Metacraton northward (see Abdelsalam et al., 2002) (Fig. 2A). This fact is partly substantiated by the general dearth of well-rounded framework grains (Fig. 8) and the rarity of sedimentary rock fragment counts (Figs. 8, 11, Appendix 1), which are expected in significantly transported/reworked sediments (Ola and Adepehin, 2017). Thus, the pre-rift crustal masses within the Sirte Basin are favored as the sources of these arenaceous sediments.

Compositionally, these pre-rift sediments sources are made up of pre-Cretaceous igneous and metamorphic basement rocks with some sedimentary and volcanic rocks around the Calanscio area (El-Hawat, 1992; Ambrose, 2000; Hallett, 2002). The quartzose/orthoquartzite ($Q_{97}F_0L_3$) nature of the Upper Sarir Sandstone Formation in the Sarir Field, is typified by the datasets in this study (Fig. 7) and does not characteristically reflect the high K-feldspar (≤35%), plagioclase (25–50%), and biotite with amphibole (≤30%) configurations expected of sediment dominantly derived igneous rocks (see Nesbitt and Young, 1984; Earle, 2019). Similarly, the current data (Figs. 8–9, 12) strongly oppose the significant diagenetic breakdown of unstable framework grains (feldspar and lithics) attributed by earlier authors to be a dominant control in arenite production (see McBride, 1985; Wahab, 1998; Garzanti, 2017). These facts suggest that sedimentological processes other than provenance impacted significant control on the quartz-richness of the formation.

5.2. Paleoclimate and weathering

The compositional signatures of the Upper Sarir Sandstone Formation suggest robust pre-depositional processes, which favored the disintegration of unstable mineral components (feldspar, biotite, and lithics) from the sediments. Although the unroofing time of the interpreted plutonic and metamorphic progenitors (see Fig. 15B) of the sandstones cannot be unequivocally ascertained, it is possible that they are pre-Cretaceous and were affected by the Jurassic to Cretaceous transition. Using the petrographic paleoclimate model of Suttner et al. (1981), the significant influence of humid climate on the sediment source massifs and perhaps the sediment before burial is depicted (Fig. 13D). Compared to arid-derived detritus, humid-sourced sediments are typically deficient in feldspar (usually less than 10–25%), although both may record SiO_2 (quartz) composition ≥ 80% (Suttner and Dutta, 1986; Akinlotan et al., 2021) (Fig. 3). As such, the general lack of unstable feldspar (≤5%) and quartz occurrence beyond the 80% threshold support a warm, humid paleoclimate condition for the Upper Sarir Sandstone Formation detritus.

The early Cretaceous paleoconditions of a warmer temperature, sea-level rise, and precipitation surge (Reyment and Dingle, 1987) alongside an increase in pCO_2 concentration were suitable conditions that instigated intense chemical disintegration of source massifs and the

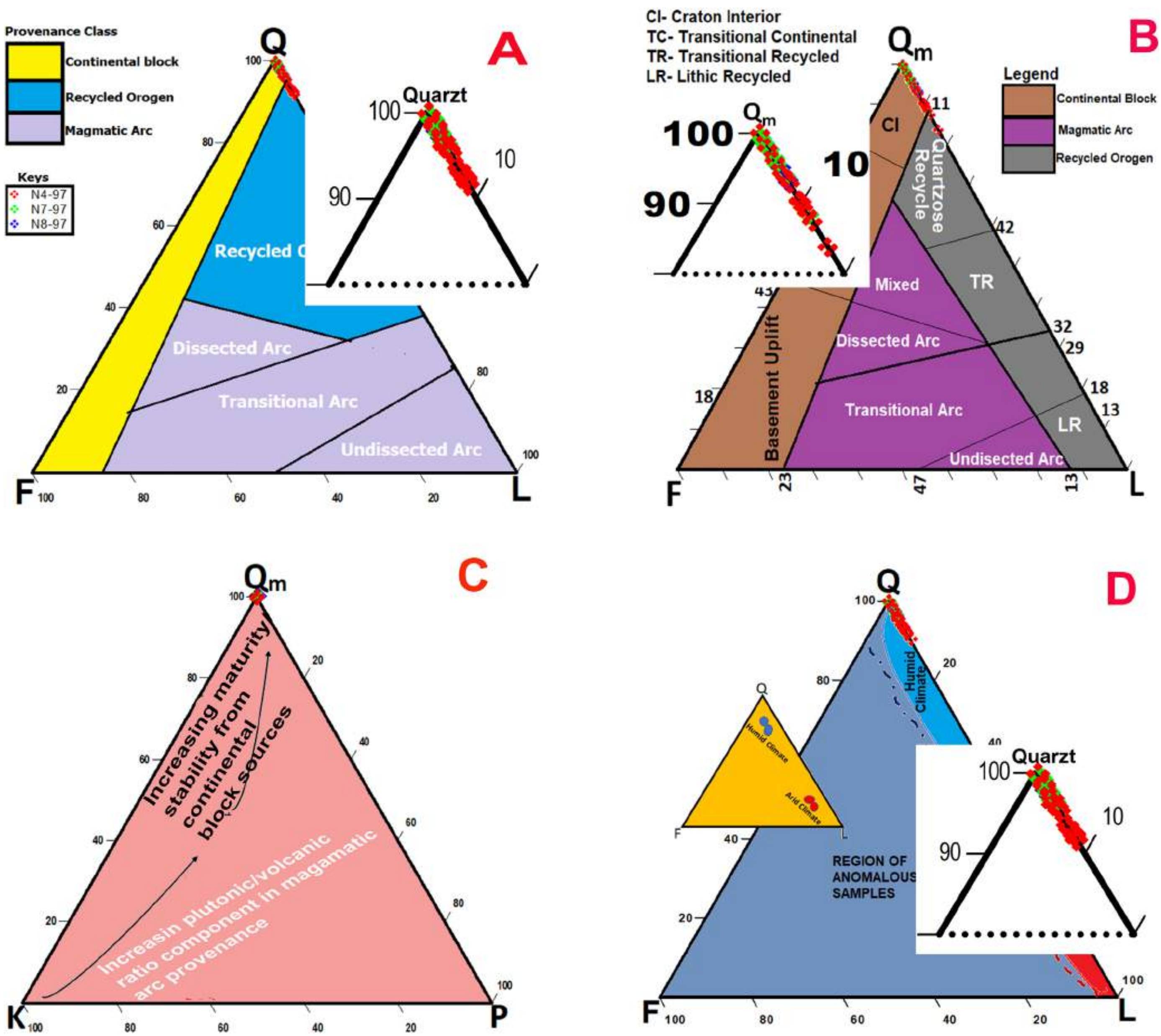

Fig. 13. Provenance and maturity indicative ternary models (Dickinson and Suczek, 1979) of the quartzose sandstones (n = 40): (A) QFL plot suggesting the dominance of craton interior and minor recycled orogenic provenance for the quartzose, (B) Q_MFL plot indicating 95% of the samples were derived from craton interior sources within the continental block, (C) Q_MKP triplot suggesting increasing maturity from continental block provenances, (D) QFL plot showing the influence of humid paleoclimate on the studied quartzose sandstones.
(After Suttner et al. (1981).)

selective destruction of unstable mineral grains, thus concentrating quartz-rich sediments that were later transported, deposited, and lithified to form quartzose (Figs. 5, 7, 8, 11). Probable geological inferences drawn from the global abundance of early Cretaceous evaporites mainly between latitudes 10° and 30°N and the rich amounts of coal poleward of 30°N have been interpreted to be indicative of arid subtropics and humid conditions around the mid-latitudes, respectively by some authors (see Drewry et al., 1974; Cao et al., 2019).

Nevertheless, the known abundances of early Cretaceous laterite/saprolite (e.g., Negev Desert, Israel) and bauxite (e.g., Um Bogma bauxite in SW Sinai, Northern Egypt) in contiguous regions of north Africa (see Fig. 2A), which are indicative of intense chemical weathering, support humid paleoclimates of source massifs (Schwarz and Germann, 1999; Avigad et al., 2005). This interpretation is strongly supported by the consistent dominance of kaolinite (see Figs. 9–11), which is interpreted as a product of intense chemical weathering in the source areas (Dudek, 2012), over other clay minerals. Regional correlation for the Cambro-Ordovician (540–455 Ma) quartzose from southern Israel by Avigad et al. (2005) shows that chemical weathering dominated not only the northern fringe of Gondwanaland in the early Cretaceous but also in the Neoproterozoic–Cambrian–Ordovician. Nevertheless, the warm and humid climate interpreted by these authors was perhaps milder than the early Cretaceous, which produced the Upper Sarir Sandstone Formation.

5.3. Sediment transport history and depositional energy

An interpreted depositional model for the studied quartzose sandstone in the Sarir Field suggests a possible short-lived and perhaps tidally influenced meandering system that was succeeded by a prolonged braided river system (Fig. 15A). Very rare dwindling of depositional energy resulted in the deposition of shale laminae (Figs. 12, 15). This agrees

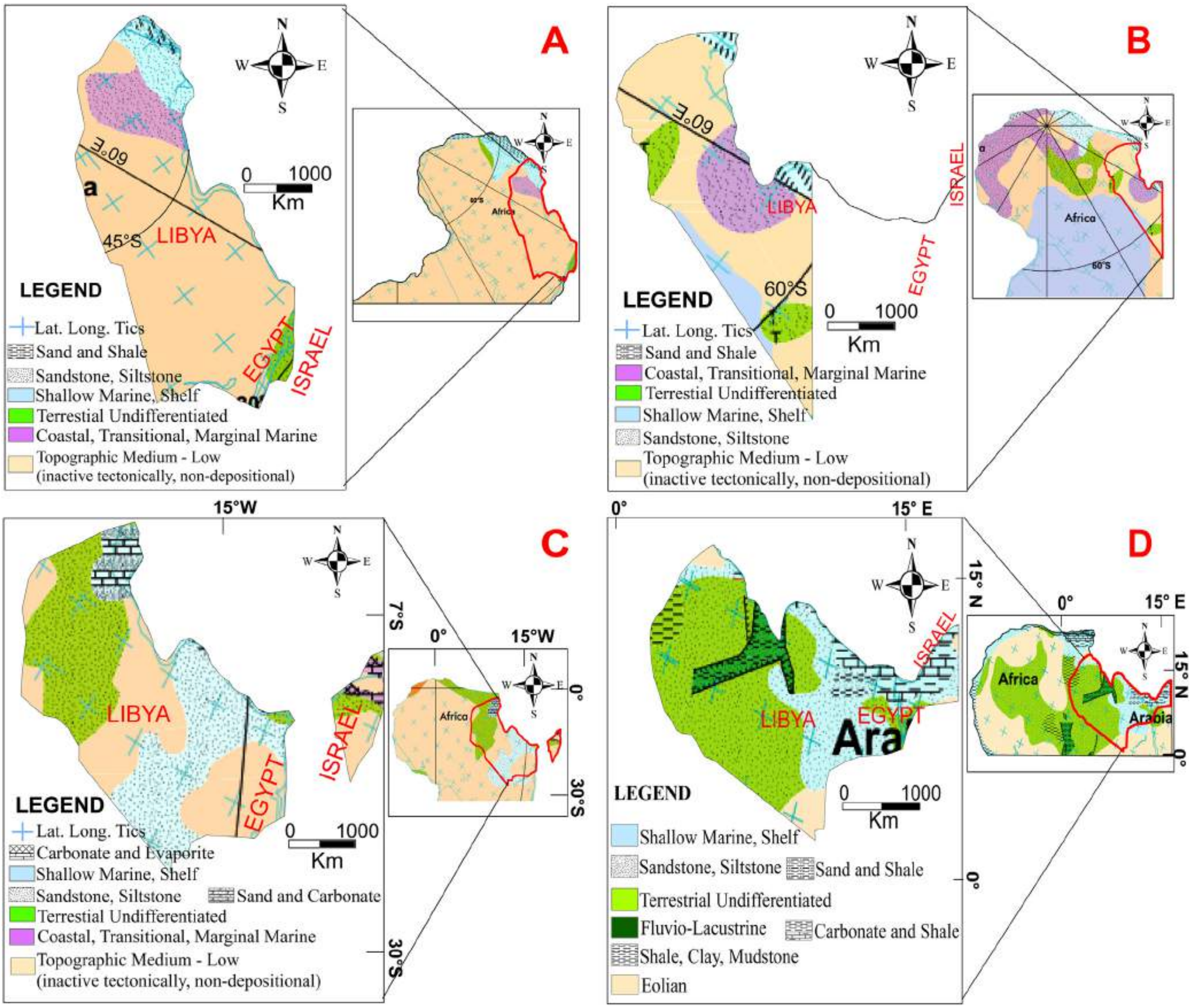

Fig. 14. Northern Gondwana (Libya, Egypt and Israel) regional paleoenvironment and paleolithofacies maps showing depositional relationship between the study area and contiguous areas in (A) Late Cambrian, (B) Late Ordovician, (C) Middle Permian, (D) Early Cretaceous.
(Adapted from Golonka (2007, 2012).)

with the multi-depositional and fluctuated sedimentation systems previously reported for the Sarir Group (e.g., El-Hawat et al., 1996; Ambrose, 2000; Weihe et al., 2008). A predominantly braided alluvial facies has been interpreted for sediments around the Hameimat Trough (El-Hawat et al. 1996), while minimum incursions of a lacustrine system, evidenced by intercalated shale have also been suggested (Weihe et al., 2008). In the Sarir region, evidence of meandering fluvial, deltaic coastal plain and tidal flat facies has been presented (Ambrose, 2000; Gras and Thusu, 1998). The sediment transportation model for the Upper Sarir Sandstone Formation indicates that the southwesterly-situated pre-rift Messla High–South Sarir High system and, to a lesser extent, the Eastern Shelf High alongside other basement highs in the SE Sirte Basin are the dominant precursors of the syn-rift Sarir Group detritus (Fig. 15B). The proximity of identified source massifs of the Upper Sarir Sandstone Formation to the depositional sites indicates a relatively short source to sink travel distance that does not exceed an average of 100 km (Fig. 15).

The conspicuously subangular to subrounded angular signature of the quartzose is testament to this short transport distance (Fig. 8). The domination of non-rounded grains and poor sorting (Figs. 7, 8) suggest the quartzose are first-cycle and non-reworked (see Ola and Adepehin, 2017). Hence, the mineralogical maturity of the sediments in this part of the Northern Gondwana could not have been occasioned by sediment recycling (Figs. 5, 9, 10, 13). The cross-bedded, unfossiliferous, and conglomeratic signatures of the quartzose sandstone of the Upper Sarir Sandstone Formation as evident on subsurface whole-cores and sidewall cores are indicators of a predominantly distal braided stream (fluvial) depositional environment (see Ibrahim, 1991; Sadeg and Haithem, 2007). Hence, these quartzarenites were probably deposited as bedload via traction and perhaps saltation. Although these processes might have contributed to the quartzose nature of the early Cretaceous sandstone, the interpreted low to high velocity of the streamflow associated with them and short to moderate travel distance, alongside the compositional signature of the quartzose all suggest the sediments were mainly eroded, transported, deposited as clean quartz-rich detritus. Thus, a warm and humid paleoclimate and its associated rigorous early Cretaceous weathering are constrained as the major sedimentological controls that shaped the compositional framework of the Upper Sarir Sandstone Formation in northern (Libya) Gondwana.

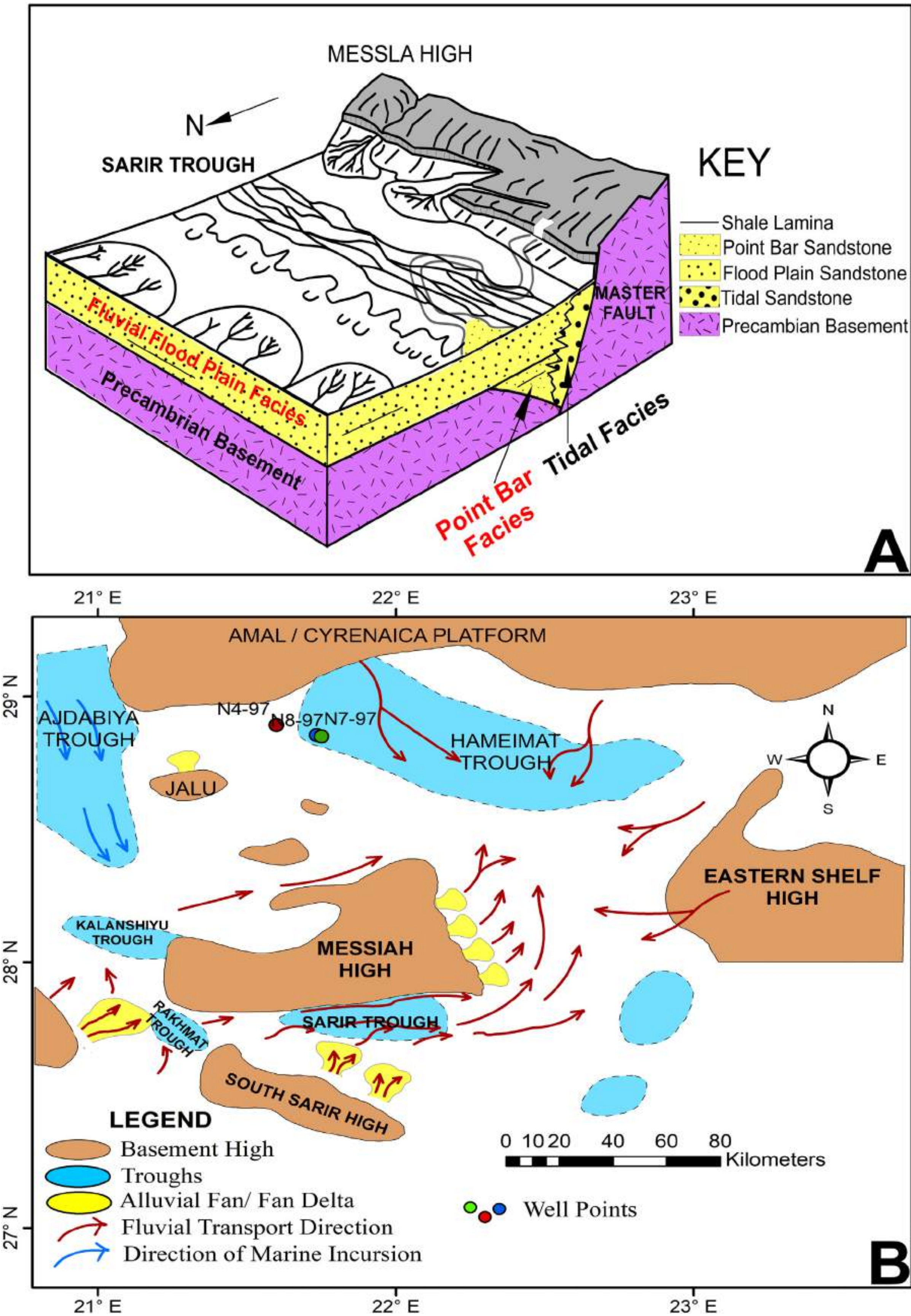

Fig. 15. Depositional model of the Upper Sarir Sandstone Formation in the Sarir Area, Sirte Basin, Libya. (A) Interpreted facies model suggesting brief tidally influenced meandering stream, and a prolonged braided fluvial river, (B) an early Cretaceous paleoflow model during the sedimentation of Upper Sarir Sandstone Formation quartzose in the Sirte Basin. (After Ambrose (2000).)

5.4. Regional paleosedimentation and paleolithofacies implications

The paleogeographic relevance of the presented data provides insights on regional depositional signatures through important geologic times in northern Gondwanaland (Fig. 14). During the late Cambrian most of the African plate was tectonically inactive and there was no deposition, except in the north (Fig. 14A). The northern reaches of Libya witnessed sedimentation of coastal-marine deposits, whereas influx of continental facies dominated the Israeli–Egyptian blocks (Klitzsch, 1990; Golonka, 2012). Generally, Africa experienced more sedimentation during the Ordovician than the Cambrian. By the mid-Ordovician, most part of Central Africa had been overlain by shallow marine deposits (Fig. 14B). Although no reliable juxtaposition can be drawn to Egypt and Israel, data from Libya show that northern Gondwana was still topographically low with no significant sedimentary influx. Sedimentary deposition was likely dominated mainly by coastal-marginal marine conditions, with pockets of terrestrial deposits in eastern and southern Libya. The formation of the Pangea in the Permian coincides with the widespread distribution of shallow marine, shelfal, and continental siltstone and sandstone across northern Gondwana, whereas shallow marine and shelf deposited sands and carbonates occupied the northernmost end of Libya (Fig. 14C). Significant reduction of marginal marine condition could be observed (compare Fig. 14A–C). The drastic increase in regional deposition of continental clastic sediments deposited primarily by a fluvio-lacustrine system (Fig. 14D), and the overall dearth of marginal marine conditions in northern Gondwana, which was well known in the Cambrian–Ordovician–Permian, supports the hypothesis of warmer temperatures in the early Cretaceous. Thus, it is theorized that early Cretaceous first cycle quartzose might also occur in other parts of northern Gondwana, subject to the interplay of differential source lithologies/provenance, source-to-sink transport distances, and depositional conditions.

6. Conclusions

The quartzose sandstone of the Upper Sarir Sandstone Formation is texturally sub-mature and mineralogically mature. The sandstones were sourced dominantly from plutonic and metamorphic source massifs, which characterize craton interior and recycled orogenic tectonic orogenic provenances. Intense chemical weathering instigated by the warm, humid paleoclimate in the early Cretaceous disintegrated the source massifs, significantly and selectively degraded unstable feldspars and rock fragments. The quartzose sandstones were probably deposited as bedload via traction and perhaps saltation in a fluvial environment; these processes might have contributed to the compositional signatures of the quartzose. Nevertheless, holistic integration of all proxies shows that the nature of the quartz-rich sediments was attained before deposition. Thus, the short to moderate travel distances support the fact that the quartzose was primarily eroded, transported, and deposited as clean quartz-rich materials. Our data show that relatively warmer humid paleoclimate produced quartzose of the Upper Sarir Sandstone Formation than the Cambro-Ordovician humid atmosphere that produced the quartzarenite lithospheric blankets in Israel and other parts of northern Africa.

Supplementary data to this article can be found online at https://doi.org/10.1016/j.sedgeo.2021.105982.

CRediT authorship contribution statement

Research was conceived and designed by EJA. Data and sample acquisition was done by MMAA. MMAA and EJA conducted laboratory analysis, EJA interpreted the laboratory analysis and wrote manuscript draft, while other authors reviewed the draft. SPL drafted maps and facies map. CAA and HJ provided general oversight on the research.

Declaration of competing interest

The authors declare that they have no known competing financial interests or personal relationships that could have appeared to influence the work reported in this paper.

Acknowledgements

Mr. Michael Ilori assisted with the improvement of figures' quality. The critical reviews and suggestions of Professors Jasper Knight and Uwe Jenchen on the earlier drafts of the manuscript provided useful insights that improved the quality of the manuscript. These efforts are appreciated with thanks.

Funding

This research did not receive any specific grant from funding agencies in the public, commercial, or not-for-profit sectors.

References

Abadi, A.M., van Wees, J., van Dijk, P.M., Cloetingh, S.A.P.L., 2008. Tectonics and subsidence evolution of the Sirte Basin, Libya. AAPG Bulletin 92, 993–1027.

Abdel-Fattah, Z.A., 2021. Fluvial architecture of the Upper Cretaceous Nubia Sandstones: an ancient example of sandy braided rivers in central Eastern Desert, Egypt. Sedimentary Geology 420, 105923. https://doi.org/10.1016/j.sedgeo.2021.105923.

Abdelsalam, M.G., Liégeois, J.P., Stern, R.J., 2002. The Saharan Metacraton. Journal of African Earth Sciences 34, 119–136.

Adepehin, E.J., 2019. Reservoir Quality Study of Oligo-Miocene Siliciclastic Sandstones in Onshore Central Sarawak, NW Borneo: Implications From Outcrops and Subsurface Datasets. National University of Malaysia (PhD Thesis, 299 pp.).

Adepehin, E.J., Ali, C.A., Zakaria, A.A., Sali, S., 2019a. Predicting fluid-flow controls in recycled orogenic sandstones: the Nyalau Formation, onshore Sarawak Basin, NW Borneo. EAGE/AAPG Workshop on Reducing Exploration Risk in Rift Basins. European Association of Geoscientists & Engineers, pp. 1–5 2019.

Adepehin, E.J., Ali, C.A., Zakaria, A.A., 2019b. Textural and petrological characteristics of possible reservoir sandstones in the onshore Balingian province, NW Borneo. AIP Conference. Proceeding. vol. 2111, pp. 1–7.

Adepehin, E.J., Ali, C.A., Zakaria, A.A., Bankole, O.M., 2019. Occurrences and characterization of textural and mineralogical heterogeneities in analogue reservoir sandstones: case study of the onshore Central Sarawak, NW Borneo. Arabian Journal of Geosciences 12, 536. https://doi.org/10.1007/s12517-019-4705-5.

Adepehin, E.J., Ali, C.A., Zakaria, A.A., Konjing, Z., 2020. Post-depositional controls on siliciclastic tight reservoirs: implications from the Oligocene Nyalau Formation (Cycle 1), onshore Central Sarawak, Borneo. Marine and Petroleum Geology 111, 786–806.

Ahfaf, M., Ali, C.A., Jamil, H., Adepehin, E.J., 2021. Pore modification mechanisms in a deeply buried non-marine sandstone. The Early Cretaceous Upper Sarir Sandstone Formation, Sirte Basin, Libya. Journal of Petroleum Science and Engineering 205, 108813. https://doi.org/10.1016/j.petrol.2021.108813.

Ahlbrandt, T.S., 2001. The Sirte Basin Province of Libya-Sirte-Zelten total petroleum system. In: Carter, L.M. (Ed.), United States Geological Survey Bulletin 2202-F. U.S. Geological Survey, Colorado, pp. 1–29.

Akinlotan, O.O., Adepehin, E.J., Rogers, G.H., Drumm, E.C., 2021. Provenance, palaeoclimate and palaeoenvironments of a non-marine Lower Cretaceous facies: petrographic evidence from the Wealden Succession. Sedimentary Geology 415, 105848. https://doi.org/10.1016/j.sedgeo.2020.105848.

Alkhazmi, R.A., 1988. Petrography of Basal "Sarir-Nubian" Sandstone at C43, C46, L2, and HHI-65, The Sarir and Messla Fields SE Sirte Basin, Libya. Unpublished AGOCO internal report.

Ambrose, G., 2000. The geology and hydrocarbon habitat of the Sarir sandstone, SE Sirt basin, Libya. Journal of Petroleum Geology 23, 165–192.

Anketell, J.M., 1996. Structural history of the Sirt Basin and its relationships to the Sabratah Basin and Cyrenaican Platform, Northern Libya. In: Salem, M.J., El-Hawat, A.S., Sbeta, A.M. (Eds.), The Geology of Sirt Basin. 2. Elsevier, Amsterdam, pp. 57–87.

Augustsson, C., 2021. Influencing factors on petrography interpretations in provenance research—a case-study review. Geosciences 11, 205. https://doi.org/10.3390/geosciences11050205.

Avigad, D., Kolodner, K., McWilliams, M., Persing, H., Weissbrod, T., 2003. Origin of northern Gondwana Cambrian sandstone revealed by detrital zircon SHRIMP dating. Geology 31, 227–230.

Avigad, D., Sandler, A., Kolodner, K., Stern, R.J., McWilliams, M., Miller, N., Beyth, M., 2005. Mass-production of Cambro–Ordovician quartz-rich sandstone as a consequence of chemical weathering of Pan-African terranes: environmental implications. Earth and Planetary Science Letters 240, 818–826.

Barron, E.J., Washington, W.M., 1985. Warm Cretaceous climates: high atmospheric CO_2 as a plausible mechanism. In: Sundquist, E.T., Broecker, W.S. (Eds.), The Carbon Cycle and Atmospheric CO_2: Natural Variations Archean to Present. Willey and Sons, Hoboken, NJ, pp. 546–553.

Basu, A., Young, S.W., Suttner, L.J., James, W.C., Mack, G.H., 1975. Re-evaluation of the use of undulatory extinction and polycrystallinity in detrital quartz for provenance interpretation. Journal of Sedimentary Research 45 (4), 873–882.
Basu, A., 1976. Petrology of Holocene fluvial sand derived from plutonic source rocks; implications to paleoclimatic interpretation. Journal of Sedimentary Research 46 (3), 694–709.
Basu, A., 1985. Influence of climate and relief on compositions of sands released at source areas. In: Zuffa, G.G. (Ed.), Provenance of Arenites. Springer, Netherlands, pp. 1–18.
Beuf, S., Biju Duval, B., De Charpal, O., Rognon, R., Bennacef, A., 1971. Les gre`s du Pale´ozoı ¨que infe´rieur auSahara. Se´dimentations et continuite´s; e´volution struc-turale d'un craton. 18. Publ. Inst. Fr. Pe´trole, Coll. Sci etTech. du Pe´trole 18, Technip ed., Paris, p. 464.
Blatt, H., 1967. Original characteristics of clastic quartz grains. Journal of Sedimentary Research 37, 401–424.
Blatt, H., Christie, J.M., 1963. Undulatory extinction in quartz of igneous and metamorphic rocks and its significance in provenance studies of sedimentary rocks. Journal of Sedimentary Research 33, 559–579.
Brindley, G.W., Brown, G., 1980. Crystal structure of clay minerals and their xray identification. Mineralogical Society Great Britain Monograph. vol. 5 (495pp.).
Cant, D., 1992. Subsurface facies analysis. In: Walker, R.G. (Ed.), Facies models, response to sea level changes. St. John's: Geological Association of Canada, pp. 27–45.
Cao, W., Williams, S., Flament, N., Zahirovic, S., Scotese, C., Müller, R.D., 2019. Palaeolatitudinal distribution of lithologic indicators of climate in a palaeogeographic framework. Geological Magazine 156, 331–354.
Caracciolo, L., 2020. Sediment generation and sediment routing systems from a quantitative provenance analysis perspective: review, application, and future development. Earth-Science Reviews 209, 103226. https://doi.org/10.1016/j.earscirev.2020.103226.
Ceriani, A., Di Giulio, A., Goldstein, R., Rossi, C., 2002. Diagenesis associated with cooling during burial: an example from Lower Cretaceous reservoir sandstones (Sirt Basin, Libya). AAPG Bulletin 86, 1573–1591.
Chamley, H., 1989. Clay formation through weathering. In: Chamley, H. (Ed.), Clay Sedimentology. Springer, Berlin, Heidelberg, pp. 21–50.
Cox, R., Lowe, D.R., 1995. A conceptual review of regional-scale controls on the composition of clastic sediment and the co-evolution of continental blocks and their sedimentary cover. Journal of Sedimentary Research 65, 1–12.
Dabbagh, M.E., Rogers, J.J., 1983. Depositional environments and tectonic significance of the Wajid Sandstone of southern Saudi Arabia. Journal of African Earth Sciences 1, 47–57.
Dickinson, W.R., 1970. Interpreting detrital modes of graywacke and arkose. Journal of Sedimentary Research 402, 695–707.
Dickinson, W.R., 1985. Interpreting provenance relations from detrital modes of sandstones. In: Zufa, G.G. (Ed.), Provenance of Arenites. Springer, Dordrecht, pp. 333–361.
Dickinson, W.R., Suczek, C.A., 1979. Plate tectonics and sandstone compositions. AAPG Bulletin 63, 2164–2182.
Dott Jr., R.H., 2003. The importance of eolian abrasion in supermature quartz sandstones and the paradox of weathering on vegetation-free landscapes. The Journal of Geology 111, 387–405.
Drewry, G.E., Ramsay, A.T.S., Smith, A.G., 1974. Climatically controlled sediments, the geomagnetic field, and trade wind belts in Phanerozoic time. The Journal of Geology 82, 531–553.
Dudek, T., 2012. Clay minerals as palaeoenvironmental indicators in the Bathonian (Middle Jurassic) ore-bearing clays from Gnaszyn, Kraków-Silesia Homocline, Poland. Acta Geologica Polonica 62, 297–305.
Earle, S., 2019. Physical Geology. 2nd edition. University of British Columbia, Victoria, B.C. (810pp.).
Eberl, D.D., 1984. Clay mineral formation and transformation in rocks and soils. Philosophical Transactions of the Royal Society of London, Series A, Mathematical and Physical Sciences 311, 241–257.
El-Hawat, A.S., 1992. The Nubian Sandstone sequence in Sirte Basin, Libya: sedimentary facies and events. In: Sadek, A. (Ed.), Geology of the Arab World Cairo University. 1, pp. 317–327.
El-Hawat, A.S., Missallati, A.A., Bezan, A.M., Taleb, T.M., 1996. The Nubian Sandstone in the Sirt Basin and its correlatives. In: Salem, M.J., El-Hawat, A.S., Sbeta, A.M. (Eds.), The Geology of Sirt Basin. 2. Elsevier, Amsterdam, pp. 3–30.
Garzanti, E., 2016. From static to dynamic provenance analysis—sedimentary upgraded. Sedimentary Geology 336, 3–13.
Garzanti, E., 2017. The Maturity Myth in sedimentology and provenance analysis. Journal of Sedimentary Research 87, 353–365.
Golonka, J., 2007. Phanerozoic paleoenvironment and paleolithofacies maps: Mesozoic. Geologia 33, 211–264.
Golonka, J., 2012. Paleozoic Paleoenvironment and Paleolithofacies Maps of Gondwana. AGH University of Science and Technology Press, Kraków, Poland (83pp.).
Gras, R., Thusu, B., 1998. Trap architecture of the early Cretaceous Sarir sandstone in the eastern Sirt basin, Libya. In: MacGregor, D.S., Moody, R.T.J., Clark-Lowes, D.D. (Eds.), Petroleum Geology of North Africa. Geological Society of London Special Publicationvol. 132, pp. 317–334.
Hallett, D., 2002. Petroleum Geology of Libya. first edition. Elsevier B.V., Amsterdam, The Netherlands (503pp.).
Hallett, D., Clark-Lowes, D., 2016. Petroleum Geology of Libya. second edition. Elsevier, Amsterdam (391pp.).
Haq, B.U., Hardenbol, J., Vail, P.R., 1988. Mesozoic and Cenozoic chronostratigraphy and cycles of sea-level change. In: Wilgus, C.K., Hastings, B.S., Posamentier, H., Wagoner, J.V., Ross, C.A., Kendall, C.G.S.C. (Eds.), SEPM Special Publicationvol. 42, pp. 71–108.
Hassan, F., 1971. "Nubia Sandstone"—uses and misuses discussion. AAPG Bulletin 55, 887–890.
Hea, J.P., 1971. Petrography of Paleozoic–Mesozoic sandstones of the southern Sirte basin, Libya. In: Gray, C. (Ed.), Symposium on the Geology of Libya. University of Libya, Tripoli, pp. 107–126.
Ibrahim, M.W., 1991. Petroleum geology of the Sirt Group sandstones, eastern Sirt Basin. In: Salem, M.J., Belaid, M.N. (Eds.), The Geology of Libya: Third Symposium on the Geology of Libya, Held at Tripoli, pp. 2757–2779.
Johnson, S.P., Kirkland, C.L., Evans, N.J., McDonald, B.J., Cutten, H.N., 2018. The complexity of sediment recycling as revealed by common Pb isotopes in K-feldspar. Geoscience Frontiers 9, 1515–1527.
Klitzsch, E., 1990. Paleogeographical development and correlation of Continental Strata (former Nubian Sandstone) in northeast Africa. Journal of African Earth Sciences (and the Middle East) 10, 199–213.
Konstantinou, A., Wirth, K.R., Vervoort, J.D., Malone, D.H., Davidson, C., Craddock, J.P., 2014. Provenance of quartz arenites of the early Paleozoic midcontinent region, USA. The Journal of Geology 122, 201–216.
Kourkoumelis, N., 2013. PowDLL, a reusable .NET component for interconverting powder diffraction data: recent developments. In: O'Neill (Ed.), DD Annual Spring Meeting 28 on Powder Diffraction, pp. 137–148.
Kroner, A., Stern, R.J., 2004. Pan-African Orogeny. Encyclopedia of Geology 1, 1–12. https://doi.org/10.1016/B0-12-369396-9/00431-7.
Lorentzen, S., Augustsson, C., Nystuen, J.P., Berndt, J., Jahren, J., Schovsbo, N.H., 2018. Provenance and sedimentary processes controlling the formation of lower Cambrian quartz arenite along the southwestern margin of Baltica. Sedimentary Geology 375, 203–217.
Lorentzen, S., Augustsson, C., Jahren, J., Nystuen, J.P., Schovsbo, N.H., 2019. Tectonic, sedimentary, and diagenetic controls on sediment maturity of lower Cambrian quartz arenite from southwestern Baltica. Basin Research 31, 1098–1120.
Mackenzie, W.S., Guilford, C., 1986. Atlas of Rock-forming Minerals in Thin Section. Longman Group Limited, England, United Kingdom (98 pp.).
McBride, E.F., 1963. A classification of common sandstones. Journal of Sedimentary Petrology 33, 664–669.
McBride, E.F., 1985. Diagenetic processes that affect provenance determinations in sandstone. In: Zufa, G.G. (Ed.), Provenance of Arenites. Springer, Dordrecht, pp. 95–113.
McKee, E.D., 1963. Origin of the Nubian and similar sandstones. Geologische Rundschau 52, 551–587.
McKosky, J.A., 1975. Quartz in Provenance Examination. University of Michigan (MSc thesis, 71 pp.).
Meinhold, G., Morton, A.C., Fanning, C.M., Frei, D., Howard, J.P., Phillips, R.J., Strogen, D., Whitham, A.G., 2011. Evidence from detrital zircons for recycling of Mesoproterozoic and Neoproterozoic crust recorded in Paleozoic and Mesozoic sandstones of southern Libya. Earth and Planetary Science Letters 312, 164–175.
Millot, G., 2013. Geology of Clays: Weathering, Sedimentology, Geochemistry. Springer Science & Business Media, Berlin (427 pp.).
Moore, D.M., Reynolds Jr., R.C., 1997. X-ray Diffraction and the Identification and Analysis of Clay Minerals. second edition. Oxford University Press, Oxford (378 pp.).
Morton, A.C., Meinhold, G., Howard, J.P., Phillips, R.J., Strogen, D., Abutarruma, Y., Elgadry, M., Thusu, B., Whitham, A.G., 2011. A heavy mineral study of sandstones from the eastern Murzuq Basin, Libya: constraints on provenance and stratigraphic correlation. Journal of African Earth Sciences 61, 308–330.
Müller, R.D., Sdrolias, M., Gaina, C., Steinberger, B., Heine, C., 2008. Long-term sea-level fluctuations driven by ocean basin dynamics. Science 319, 1357–1362.
Nazeer, A., Abbasi, S.A., Solangi, S.H., 2016. Sedimentary facies interpretation of Gamma Ray (GR) log as basic well logs in Central and Lower Indus Basin of Pakistan. Geodesy and Geodynamics 7, 432–443.
Nesbitt, H.W., Young, G.M., 1984. Prediction of some weathering trends of plutonic and volcanic rocks based on thermodynamic and kinetic considerations. Geochimica et Cosmochimica Acta 48, 1523–1534.
Ola, P.S., Adepehin, E.J., 2017. Sedimentological interpretation of coastal ditch cuttings: implications for subsurface geology and Provenance in Dahomey Basin, Nigeria. Arabian Journal of Geosciences 10. https://doi.org/10.1007/s12517-016-2821-z.
Pettijohn, F.J., Potter, P.E., Siever, R., 1987. Introduction and source materials. In: Pettijohn, F.J., Potter, P.E., Siever, R. (Eds.), Sand and Sandstone. Springer, New York, pp. 1–21.
Pomeyrol, R., 1968. Nubian sandstone. AAPG Bulletin 52, 589–600.
Potter, P.E., 1978. Petrology and chemistry of modern big river sands. The Journal of Geology 86, 423–449.
Poulsen, C.J., Gendaszek, A.S., Jacob, R.L., 2003. Did the rifting of the Atlantic Ocean cause the Cretaceous thermal maximum? Geology 31, 115–118.
Radwan, A.E., 2021. Modeling the depositional environment of the sandstone reservoir in the Middle Miocene Sidri Member, Badri Field, Gulf of Suez Basin, Egypt: integration of gamma-ray log patterns and petrographic characteristics of lithology. Natural Resources Research 30, 431–449.
Reyment, R.A., Dingle, R.V., 1987. Palaeogeography of Africa during the Cretaceous period. Palaeogeography, Palaeoclimatology, Palaeoecology 59, 93–116.
Rothman, D.H., 2002. Atmospheric carbon dioxide levels for the last 500 million years. Proceedings of the National Academy of Sciences 99, 4167–4171.
Sadeg, E.B.H., Haithem, M.A., 2007. Facies and petrophysical analysis of Nubian reservoir, Rimal oil field–Sirte basin. The Fifth International Conference on the Geology of Africa, Assiut, Egypt 1, pp. 51–70.
Schwarz, T., Germann, K., 1999. Weathering surfaces, laterite-derived sediments and associated mineral deposits in north-east Africa. In: Thiry, M., Simon-Coincon, R. (Eds.), Palaeoweathering, Palaeosurfaces and Related Continental Deposits. International Association of Sedimentologists Special Publication, Gent, Belgiumvol. 27, pp. 367–390.
Scotese, C.R., 2014. Atlas of Early Cretaceous paleogeographic maps. In: Scotese, C.R. (Ed.), The Cretaceous Maps, Mollweide Projection. PALEOMAP Atlas for ArcGIS, Evanston, ILvol. 2, pp. 23–31.

Selley, R.C., 1968. Near-shore marine and continental sediments of the Sirte basin, Libya. Quarterly Journal of the Geological Society 124 (1-4), 419–460.
Selley, R.C., 1972. Diagnosis of marine and non-marine environments from the Cambro-Ordovician sandstones of Jordan. Journal of the Geological Society 128, 135–150.
Selley, R.C., 1997. Sirte Basin of Libya-the sedimentary basins of northwest Africa: stratigraphy and sedimentation. In: Selley, R.C. (Ed.), Sedimentary Basins of the World. Elsevier, Amsterdam, pp. 3–16.
Sladen, C.P., Batten, D.J., 1984. Source-area environments of Late Jurassic and Early Cretaceous sediments in southeast England. Proceedings of the Geologists' Association 95, 149–163.
Suttner, L.J., Dutta, P.K., 1986. Alluvial sandstone composition and paleoclimate; I, framework mineralogy. Journal of Sedimentary Research 56, 329–345.
Suttner, L.J., Basu, A., Mack, G.H., 1981. Climate and the origin of quartz arenites. Journal of Sedimentary Research 51, 1235–1246.
Wahab, A.A., 1998. Diagenetic history of Cambrian quartz arenites, Ras Dib-Zeit Bay area, Gulf of Suez, eastern desert, Egypt. Sedimentary Geology 121, 121–140.
Weihe, T., Porebski, S.J., Dellepiane, S., 2008. Hameimāt Trough, East Sirt Basin, Libya. Geology 1, 187–200.